frontiers | Frontiers in Marine Science

TYPE Original Research
PUBLISHED 21 November 2023
DOI 10.3389/fmars.2023.1293893

OPEN ACCESS

EDITED BY
Feng Pan,
Xiamen University, China

REVIEWED BY
Mao-Xu Zhu,
Ocean University of China, China
Wytze Lenstra,
Radboud University, Netherlands

*CORRESPONDENCE
Darci A. Swenson Perger
darci.swenson@stonybrook.edu

RECEIVED 13 September 2023
ACCEPTED 30 October 2023
PUBLISHED 21 November 2023

CITATION
Swenson Perger DA, Dwyer IP, Aller RC, Volkenborn N, Heilbrun C and Wehrmann LM (2023) Seasonal iron fluxes and iron cycling in sandy bioirrigated sediments.
Front. Mar. Sci. 10:1293893.
doi: 10.3389/fmars.2023.1293893

Seasonal iron fluxes and iron cycling in sandy bioirrigated sediments

Darci A. Swenson Perger*, Ian P. Dwyer, Robert C. Aller, Nils Volkenborn, Christina Heilbrun and Laura M. Wehrmann

Stony Brook University, School of Marine and Atmospheric Sciences, Stony Brook, NY, United States

Permeable sediments, which represent more than 50% of the continental shelves, have been largely neglected as a potential source of Fe in current global estimates of benthic dissolved iron (Fe_d) fluxes. There are open questions regarding the effects of a range of factors on Fe_d fluxes from these deposits, including seasonal dynamics and the role of bioirrigation. To address these gaps, we performed laboratory-based sediment incubation experiments with muddy sands during summer (21 °C) and winter (7 °C). We used bioirrigation mimics to inject overlying water into the permeable sediment with patterns resembling the bioirrigation activity of the prolific bioturbating polychaete, *Clymenella torquata*. Newly developed in-line Fe accumulators were used to estimate Fe fluxes with a recirculating set-up. We found high Fe_d fluxes from sandy sediments, especially in benthic chambers with simulated bioirrigation. In the winter fluxes reached >200 μmol Fe_d m^{-2} d^{-1} at the onset of irrigation and then decreased over the course of a 13-day experiment while in the summer fluxes from irrigated sediments reached >100 μmol Fe_d m^{-2} d^{-1} and remained high throughout a 7-day experiment. Despite different geochemical expressions of Fe-S cycling and resulting porewater Fe_d concentrations in winter and summer, large Fe_d fluxes were sustained during both seasons. Solid-phase and porewater concentration profiles showed that maximum concentrations of key constituents, including total solid-phase reactive Fe, and porewater Fe_d and ammonium, were located closer to the sediment water interface (SWI) in irrigated cores than in non-irrigated cores due to the upward advective transport of dissolved porewater constituents. This upward transport also facilitated Fe_d fluxes out of the sediments, especially during times of active pumping. Our study demonstrates the potential for large Fe_d fluxes from sandy sediments in both summer and winter, despite relatively low standing stocks of labile organic matter and porewater Fe_d. The primary driver of these high fluxes was advective porewater transport, in our study induced by the activity of infaunal organisms. These results suggest that permeable sediments, which dominate shelf regions, must be explicitly considered in global estimates of benthic Fe_d fluxes, and cannot be simply extrapolated from estimates based on muddy sediments.

KEYWORDS

permeable sediments, iron, benthic flux, bioadvection, bioirrigation, biogeochemistry

1 Introduction

Iron (Fe) is a redox sensitive metal that is a critically important nutrient, but often limiting in the ocean (Martin and Fitzwater, 1988; Behrenfeld et al., 1996; Coale et al., 1996; Behrenfeld and Kolber, 1999) due to its low solubility at current ocean pH and oxygen (O_2) concentration (Millero et al., 1995). Continental margin sediments are suggested to be an important source of dissolved Fe (Fe_d, operationally defined as Fe that can pass through a 0.2 µm filter) to the ocean (Elrod et al., 2004; Conway and John, 2014), though current flux estimates are not well constrained (Dale et al., 2015). By relating Fe fluxes to organic carbon oxidation, Elrod et al. (2004) estimated the global continental shelf benthic flux to be approximately 89 Gmol y^{-1} (~ 4.3 µmol m^{-2} d^{-1}). Dale et al. (2015) later used a model that included both organic carbon oxidation and bottom water oxygen concentrations to estimate a continental shelf benthic Fe flux of 109 ± 55 Gmol y^{-1}(~5.3 µmol m^{-2} d^{-1}). There are still components that are not resolved in the model, including seasonal and species-specific variability in benthic macrofaunal activity, such as differences in irrigation mechanisms and pumping rates, that cannot be captured by single constants. Additionally, these models were based on a limited set of data, most of which were collected off the California margin (Dale et al., 2015). As a result, the global Fe_d benthic flux was extrapolated assuming muddy diffusive sediments, and failed to consider sandy advective sediments, which make up ~ 50% of continental shelves (Huettel et al., 2014).

Early diagenetic processes in marine sediments play a key role in controlling the benthic fluxes across the sediment water interface (SWI). Within sediments, various electron acceptors are utilized in the remineralization of organic carbon (C_{org}), typically used in the order of most energetically favorable to least energetically favorable, following the pattern of O_2, nitrate (NO_3^-), Mn-oxides, Fe-oxides, sulfate (SO_4^{2-}), and carbon dioxide (CO_2) with depth (Froelich et al., 1979). The Fe-oxides are reduced during dissimilatory iron reduction (DIR) and can also be reduced during the reoxidation of hydrogen sulfide (H_2S), the product of sulfate reduction (Millero, 1991; Poulton et al., 2004). Both processes release Fe_d into the surrounding porewater that can then diffuse deeper into the sediments or undergo secondary reactions that retain it in the sediment. Diffusing Fe_d can move towards the SWI and may ultimately escape from the sediment as a benthic Fe_d flux. Secondary processes of the released Fe_d include reaction with H_2S at depth to form iron-sulfur minerals, such as iron monosulfides (FeS) and pyrite (FeS_2) (Rickard, 2006; Rickard and Luther, 2007; Scholz et al., 2014; Lenstra et al., 2021) and reoxidation to Fe-oxides by O_2, NO_3^-, or Mn-oxides (Lovley and Phillips, 1988) near the SWI. The formation of iron-sulfur minerals can result in the more permanent burial of Fe (and sulfur) in the sediments (Berner, 1970). Alteration of sediment redox conditions, however, can result in the reoxidation of Fe sulfides and the return of Fe back into the reactive Fe-oxide pool (i.e. Fe that readily reacts with sulfide) (Canfield, 1989; Schippers and Jørgensen, 2001; Rickard and Luther, 2007). During reoxidation, Fe_d can again be generated as an intermediate product (Aller, 1980; Nielsen and Risgaard-Petersen, 2015). The input of organic material, which varies seasonally, therefore has a critical influence on the sedimentary oxygen dynamics, Fe cycling and resulting benthic Fe_d fluxes on continental margins.

Much of the research investigating sedimentary Fe cycling has been done in muddy organic-rich cohesive sediments, where molecular diffusion is the dominant transport process within the sediments, though exchange of solutes between the sediments and overlying water can be enhanced by the flushing of burrows into which reduced metabolite can diffuse along concentration gradients (Severmann et al., 2010; Lenstra et al., 2019). Permeable sediments, defined by a permeability of ≥ 10^{-12} m^2 (~1 darcy) (Wilson et al., 2008; Huettel et al., 2014) have been shown to be sites of significant C_{org} remineralization (Boudreau et al., 2001; de Beer et al., 2005; Huettel et al., 2014), with C_{org} remineralization rates similar to those of muddy cohesive sediments despite low standing stocks of organic matter (Rowe et al., 1988). The supply of organic matter and oxygen and the removal of remineralization products by advective porewater flow are considered to be the main drivers of efficient organic matter mineralization in permeable sediments. Porewater advection is driven by pressure gradients that can be caused by tidal currents, wave action, and the interaction of bottom currents with physical and biological structures (Forster et al., 1996; Huettel and Rusch, 2000; D'Andrea et al., 2002; Precht et al., 2004; Reimers et al., 2004; Santos et al., 2012) and also by the activities of benthic macrofaunal organisms (Wethey et al., 2008). The advective flow of porewater can transport oxygen and C_{org} up to at least several centimeters into the sediment (Huettel et al., 1996; Huettel and Rusch, 2000), while also quickly flushing out accumulated remineralization products, including ammonium (NH_4^+) and dissolved inorganic carbon (DIC), effectively allowing the sediment to act as a biocatalytic filter (Huettel and Rusch, 2000). The benthic cycling of Fe_d in sandy sediment and the scale and controlling factors of Fe_d fluxes in this environment remain little investigated, though previous work suggests advective transport coupled to Fe remobilization processes can be important drivers of benthic fluxes from permeable sediments (Huettel et al., 1998; Jahnke et al., 2005).

Bioirrigation describes the transport of water into, through and out of the sediment by the burrow ventilation of benthic macrofauna. It has been shown to greatly increase the exchange of solutes between porewater and overlying water relative to what would be observed solely through molecular diffusion (Aller, 2001) in sediments, especially in permeable sands (Kristensen and Kostka, 2005; Meysman et al., 2006; Volkenborn et al., 2007a; Volkenborn et al., 2007b; Huettel et al., 2014). Bioirrigators affect the biogeochemistry of the sediment by injecting oxygen-rich overlying water into the burrow, which influences the redox conditions of the surrounding sediments by flushing out remineralization products (Davis, 1974; Volkenborn et al., 2012) and enhancing the reoxidation of Fe^{2+} and Fe sulfides (van de Velde and Meysman, 2016). The extent of bioirrigation is dependent on a number of factors, varying greatly among species, burrow types, and the intended function of the burrow ventilation (e.g. if irrigation predominately supports suspension-feeding, metabolite flushing, or some combination of both) (Aller, 1982; Kristensen, 2001; Kristensen and Kostka, 2005; Volkenborn et al., 2012).

In this study, we aimed to evaluate the effect of bioirrigation and seasonality on Fe cycling and Fe_d fluxes from sandy sediments. Over a 9-month period, key iron-cycling parameters were assessed from sampling an intertidal sandflat on the south shore of Long Island, NY, densely populated by the maldanid polychaete, *Clymenella*

torquata. Sediment incubation experiments with and without bioirrigation mimics were conducted using sediments collected in the summer and winter. Bioirrigation mimics were designed to accurately reflect *in situ* irrigation patterns by benthos and population densities common in the study area (Dwyer et al., in review). Fe_d fluxes were estimated using the in-line Fe accumulators as described by Aller et al. (2023) and porewater profiles and solid-phase compositions were compared across seasons. This study provides some of the first benthic Fe_d flux estimates from bioirrigated sands, isolating the effect of bioadvection, and closing an important gap in our knowledge of the potential for permeable sands to act as a significant source of Fe_d to the ocean.

2 Materials and methods

2.1 Sediment collection

2.1.1 Sediment collection for reactive Fe-oxide field monitoring

Sediment was collected monthly, from July 2021 to April 2022, at an intertidal sand flat adjacent to Ponquogue Bridge in Shinnecock Bay, Long Island, New York (Figure 1) for monitoring Fe-speciation in solid-phase samples. Sediments were collected at low-tide while overlying water was absent. Polycarbonate tubes (~9.5 cm diameter) were used to collect the upper 15 cm of sediment. Cores were immediately sampled at coarse intervals, including a surface scraping of approximately 0.2 cm, and from the top 1 cm, 1-6 cm, and 6-15 cm. Samples were placed in plastic bags and immediately put in a cooler with ice, and frozen upon return to the lab. Sediment was sampled from 2-3 cores collected from two locations (Figure 1) in the low intertidal densely populated by *C. torquata* (approximately 1000-3000 indviduals m^{-2}) and in the high intertidal that was only sparsely populated by *C. torquata* (approximately 0-400 individuals m^{-2}). Samples were analyzed only for operational Fe-oxide content following the procedure described in 2.6.1.

2.1.2 Sediment collection for incubation experiment

Sediment incubation experiments were performed using sediment collected from the intertidal sand flat described in 2.1.1 during low-tide. Sediments at this site are composed of muddy sand, with a measured porosity of ~0.44 and with a permeability of ~1.6 $x10^{-11}$ (16.2 darcys). Polycarbonate tubes were used to collect the upper ~15 cm of sediment during low tide in September

FIGURE 1
Satellite map (Map data: Google, SIO, NOAA, U.S. Navy, NGA, GEBCO, LDEO-Columbia, NSF, NOAA, U.S. Geological Survey; Map data: Google, SIO, NOAA, U.S. Navy, NGA, GEBCO) showing the sediment collection sites #1 and #2 (depicted by red stars) in Shinnecock Bay (outlined in red) on the south shore of Long Island, NY. Scale bars in the bottom right corners for location size reference.

2020 (water temperature ranging from 19-22 C, Salintity was ~ 30 psu) for the summer experiment and in January 2021 for the winter experiment (water temperature ranging from 2-8 C, Salintity was ~ 33 psu). Cores were collected in polycarbonate tubes, sealed, and placed in buckets filled with seawater before being transported back to the lab for processing. This mode of core transport maintained core structure and avoided porewater drainage until sampling or additional processing.

2.2 Incubation experiment with irrigation mimic set-up

The following procedure was carried out for both summer and winter microcosm experiments. All chambers, tubing, and connectors were acid cleaned (10% trace metal grade HCl) prior to starting the experiments. In the lab, cores were sliced into 3 depth sections: the top 0-1 cm, the middle 1-6 cm, and the bottom 6-15 cm. Each section was collected into a bucket and homogenized by hand, then sieved through a 2 mm sieve to remove large macrofauna. The sieved sediment was used to fill seven polycarbonate cylindrical chambers (~14.6 cm diameter) by redistributing the sections of sediments successively. Chambers were filled first with 9 cm of "bottom" sediment, then 5 cm of "middle sediment", and topped with 1 cm of "top" sediment. Three smaller polycarbonate tubes (~9.5 cm diameter) were filled in the same way and placed in large buckets filled with seawater to prevent atmospheric exposure. These "initial cores" were sampled for porewater and solid-phase sediment after 24 in the winter and after 48 hours in the summer to get baseline measurements for the sediment columns.

Each experimental chamber was then filled gently with ~12 cm of overlying seawater and sealed with a polycarbonate cap. There were two polycarbonate chambers with only seawater (~1800 mL, no sediment) which were used as control cores. Each cap was fitted with inflow and outflow ports, which were part of a recirculation system with peristaltic pumps (Masterflex 7550-50) that continuously exchanged the overlying water at a rate of 32 mL min^{-1} in the winter (τ ~1 hr) and between 32-64 mL min^{-1} in the summer (τ ~0.5-1 hr) between the chambers and individual 4-liter reservoirs. Chamber outflow was continuously monitored for dissolved O_2 in a subset of cores using Pyroscience (Pyroscience TSUB36 Shielded Submersible Temperature Sensors, Pyroscience OXFTC2 Oxygen Flow-Through Cells, and Pyroscience SPFIB-BARE-CL2 Optical Fibers) and PreSens (PreSens PT100 Temperature Sensor, PreSens POF-FTC-L2.5-1ST optical fibers, and Presens FTC-PSt7-10-YOP-4mm Flow Through Cells for Oxygen) sensors to ensure fully oxic conditions in the overlying water and water exchange rate was adjusted, if necessary. The lid also held a magnetic stir bar, and motors with rotating magnets were used to rotate the sir bars in a pre-set pattern of 15 sec stirring, 15 sec rest, 15 sec stirring in the opposite direction, and 15 sec rest that was found to limit physical artifacts caused by stirring (Janssen et al., 2005). Each circulation system was fitted with an in-line Fe accumulator attached to the outflow tubing (Aller et al., 2023). The Fe accumulators were comprised of 2 g of glass wool (Pyrex C3950, 8 µm diameter) filled loosely in a 50 mL centrifuge tube with the bottom cut open. Fe accumulators were placed vertically in the lid of the individual reservoirs, allowing water to flow through the glass wool and return to the reservoir while trapping Fe_d, Fe^{3+} chelates, and other forms of particulate Fe (Aller et al., 2023) in the process. Air stones connected to air pumps were used to fully reoxygenate the water after it had passed through the Fe accumulator and before being circulated back into chambers. Fe accumulators were exchanged at predetermined time intervals, generally ~24 hrs, with exact timing recorded.

Experimental cores were exposed to one of two treatments (Figure 2 and Supplemental S2). Four of the cores were designed to mimic the bioirrigation patterns of *Clymenella torquata*, an infaunal polychaete that orients head-down and injects oxic water at depth into a blind-ended tube, creating continuously and/or intermittently oxic zones around its feeding pocket (Rhoads and Stanley, 1965; Dobbs and Whitlatch, 1982; Meysman et al., 2006). *Clymenella* is the dominant macrofauna on the sand-flat where the sediment was collected. In this set-up, the bottoms of the 4 "irrigated" cores were fitted with mesh covered injection ports (Masterflex 7014-20 pump head) that were connected by Masterflex L/S silicone tubing to computer-controlled peristaltic pumps (Masterflex 7550-50). The injection lines were connected to the circulation systems of the cores and drew water from the overlying water effluent ports. Water was injected at a rate of 0.39 mL min^{-1} [which equates to a volume pumped by ~10 individual maldanids (Mangum, 1964)] at approximately 12 cm below the sediment surface in constant time intervals, aiming to deliver water with irrigation patterns and time scales comparable to natural to patterns observed for *C. torquata*. For summer sediment and temperature conditions, this pattern was found to be 3.75 minutes of active pumping, followed by 3.75 minutes of rest, while the winter pattern was 10 minutes of active pumping, followed by 10 minutes of rest (Dwyer et al., in review). Irrigation began on Day 4 in the winter and Day 3 in the summer. Given the porosity of the sediment (0.44) and the dimensions of the cores (~15 cm sediment height, 14.6 cm diameter), the cores had an approximate porewater volume of 1100 mL. In both seasons the porewater turnover time from the addition of water during irrigation was ~4 days. The other 3 experimental cores, termed the "non-irrigated" treatment, had a standard core bottom without injection ports.

Irrigation in the cores and collection of the Fe accumulators for Fe flux estimates was not started until 3-4 days after cores were constructed to ensure a sufficient amount of time to pass to allow cores to return to their anoxic states without artifacts from core construction.

2.3 Core sampling

Upon completion of the incubation period, porewater was sampled using 5 cm long Rhizons (Rhizosphere Research Products) that were inserted horizontally through pre-drilled ports at 1 to 2 cm intervals down to the bottom of the cores (Seeberg-Elverfeldt et al., 2005; Steiner et al., 2018). To prevent oxidation of porewater analytes, Rhizons were deoxygenated in N_2-

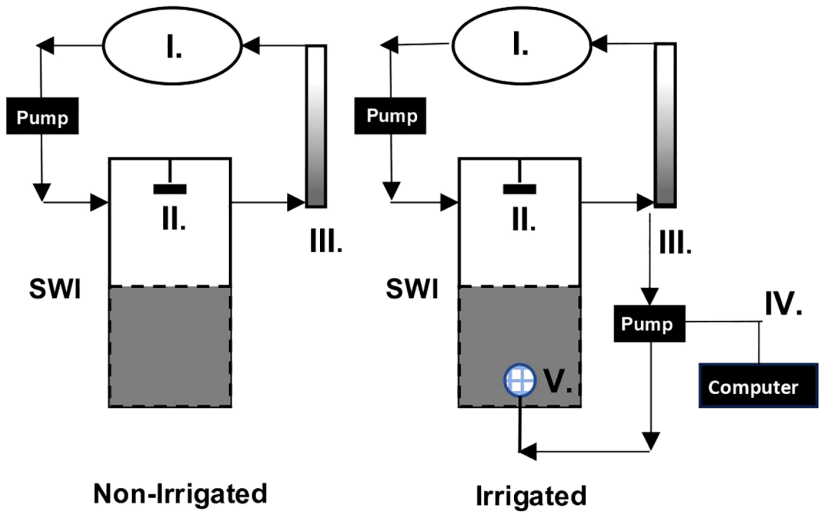

FIGURE 2
Diagram of experimental flowthrough chamber with reservoir (I), stirring mechanism (II) and Fe-accumulator (III) (Modified from Aller et al., 2023). Water flow is indicated by black arrows. The Non-Irrigated treatment is shown on the left, and the Irrigated treatment, also fitted with a mechanical irrigation mimic comprised of a computer controlled peristaltic pump (IV) and mesh covered injection port (V) is shown on the right.

bubbled water for 20 minutes prior to use. The first 0.5 mL of liquid was discarded. An aliquot of the porewater was preserved with 2% (w/v) zinc acetate for sulfide and anion (sulfate, chloride) concentration analyses. A second aliquot was acidified to 2% (v/v) with concentrated trace metal grade nitric acid for trace metal concentration analyses and stored in an acid-washed vial. A final aliquot was left untreated for analysis of ammonium concentration and alkalinity.

Subsequently, cores were drained of overlying water and prepared for solid phase sample collection. Using a clean plastic spoon, the top 2-3 millimeters of sediment were scraped off and collected separately. Sediment was then sampled in 1 cm intervals down to 3 cm (summer) and 4 cm (winter), and in 2 cm intervals below. In the irrigated treatment cores, sediment samples were taken from the bulk sediment surrounding the oxygenated pocket that formed during the experiment, as well as from within the oxygenated pocket. Samples from each depth were collected quickly after slicing under normal atmospheric conditions, put into bags and immediately frozen for later analysis.

2.4 Iron flux estimates

Fe was extracted from Fe-accumulators in a 0.5 N HCl leach for 7.5 hrs. Leachate was sampled using a syringe, filtered through 0.2 µm filter polyethersulfonate syringe filter and collected in a new vial. After leachates were sampled, the accumulators were rinsed with Milli-Q water and dried in their extraction tubes to remove any excess liquid. Extraction tubes were weighed before and after the addition of HCl and after the drying step to get an exact extraction volume. Leachates were analyzed spectrophotometrically for Fe following the ferrozine method (Stookey, 1970). Total Fe contents on the accumulators was calculated using the measured Fe concentrations and using the calculated extraction volumes. Benthic Fe_d fluxes were calculated by dividing the Fe contents extracted from the accumulators by the amount of time the accumulators were deployed and by the sediment surface area (0.167 cm^2).

2.5 Porewater analyses

The acidified pore water aliquots were diluted 1:20 with 2% trace metal grade nitric acid and analyzed for Fe_d on an Agilent 7500 inductively-coupled mass spectrometer (ICP-MS) at SUNY Stony Brook using CASS-5 as external standard, with a detection limit of 0.7 nM. Sulfide concentrations were measured spectrophotometrically on the ZnAc fixed samples diluted 2-30 fold following the Cline method (1969). Chloride and sulfate concentrations were measured on a Metrohm 930 Compact IC Flex (Metrohm A Supp 5 column, 20 µL loop, 3.2 mM Na_2CO_3/1 mM $NaHCO_3$) equipped with a Metrohm 850 Conductivity Detector and a Metrosep A PCC HC for matrix elimination using the ZnAc fixed samples diluted 1:200 fold. Standards for IC analysis were prepared from a Metrohm ISO certified sulfate and chloride standard solutions (1000 ± 5 ppm SO_4^{2-}; 1000 ± 5 ppm Cl^-) with IAPSO seawater as a secondary reference standard. Ammonium was measured colorimetrically on unfixed aliquots (Solorzano, 1969). Alkalinity was measured colorimetrically following a modified version of the method described in Sarazin et al. (1999).

2.6 Solid phase analysis

For all solid-phase analyses, samples from one core per treatment were analyzed. Prior to each analysis, the outer

oxidized surface layer was removed to avoid any reoxidation artifacts due to sample storage.

2.6.1 Reactive Fe-oxides

For each analyzed sample, between 0.25-0.35 g of frozen sediment was weighed into 15 mL centrifuge tubes for a two-step sequential reactive Fe extraction. The first step targeted labile-Fe, including amorphous Fe(III)-oxides, FeS, and non-sulfidized particulate Fe(II) (Kostka and Luther, 1994). Sediments were extracted in cold 0.5 N trace metal grade HCl for 1 hr on a shaking table. The vials were then centrifuged at 5000 rpm for 5 min. The supernatant was collected using a pipette and saved for Fe analysis. HCl supernatant (Fe_{HCl}) was analyzed for both ferrous Fe and total Fe following the ferrozine method with and without hydroxylamine hydrochloride, respectively (Stookey, 1970; Viollier et al., 2000). Fe(III) was calculated as the difference between total Fe and Fe(II). The second step was a dithionite extraction (50 g L^{-1} sodium dithionite with 0.35 M acetic acid and 0.2 M sodium citrate, buffered to pH=4.8), targeting more crystalline Fe(III)-oxides, as described in Poulton and Canfield (2005). The dithionite solution was added to each tube and the tubes were shaken for 2 hrs. The vials were centrifuged at 5000 rpm for 5 min and the supernatant was collected using a pipette. The dithionite fraction (Fe_{Dith}) was analyzed for total Fe using the Ferrozine method (Stookey, 1970). We define highly reactive Fe as the sum of $Fe(II)_{HCl}$, $Fe(III)_{HCl}$, Fe_{Dith} and Fe_{Pyrite}. Relative contribution of $Fe(II)_{HCl}$, $Fe(III)_{HCl}$, Fe_{Dith}, and Fe_{Pyrite} pools to the highly reactive Fe inventory were calculated.

We define residual reactive Fe-oxides as the sum of $Fe(III)_{HCl}$ and Fe_{Dith}. Residual reactive Fe-oxide inventories for each core interval were calculated using Equation 1, where the wet density was determined to be 1.9 g cm^{-3} and $C_{Fe\text{-}oxide}$ is the residual reactive Fe-oxide content in μmol Fe g^{-1} dry sediment.

Eq1:

$$Inventory = C_{Fe-oxide} * \frac{dry\ \ weight}{wet\ \ weight} * density_{wet} * depth\ \ interval$$

2.6.2 Acid volatile sulfide and chromium reducible sulfur

Solid sediment was analyzed for acid volatile sulfide (AVS) and chromium reducible sulfur following the distillation method described by Fossing and Jørgensen (1989). Approximately 1.5-2.5 g of frozen sediment was weighed into reaction vessels, taking care to scrape away any obviously oxidized sediment. Sediments were covered in N_2-bubbled 50% ethanol to prevent oxidation of sediment prior to the distillation. The first step of the distillation (AVS) used 6N HCl for 60 minutes while in the second step a boiling chromium chloride solution was added. The sulfur released from both distillations was collected in individual zinc acetate (5%) traps as ZnS. Traps for AVS and CRS were analyzed spectrophotometrically at 670 nm following the Cline method (Cline, 1969). Repeated analyses of NIST SRM 1646a as reference standard for CRS gave a precision of 4%. Fe_{pyrite} for each sample was calculated stoichiometrically from its CRS contents, assuming a 1:2 ratio of Fe:S.

2.6.3 Total organic carbon

Approximately 7 mg of dried sediment from the winter and summer initial cores was weighed into silver capsules and analyzed for total organic carbon (TOC). 100 μL of distilled water were added to each sample capsule, and then samples were decarbonated by fumigation in a glass desiccation chamber for 24 hours with 50 mL of 35% HCl. Samples were then placed in a Costech "zero blank" autosampler and analyzed for C content on a Thermo Scientific Isolink elemental analyzer coupled to a Delta V Plus isotope ratio mass spectrometer. Replicates of Carrera marble were measured as a TOC blank.

3 Results

3.1 Summer and winter core incubation experiments

3.1.1 Porewater chemical composition

In the winter experiment, Fe_d was present throughout the sampled sediment depths in the irrigated cores, reaching maximum concentrations of ~250 μM at ~2 cm, and decreased below, but remained >100 μM at 10 cm. In the winter non-irrigated cores, Fe_d concentrations increased to >300 μM at 2 cm, remained relatively constant from 2 cm to 7.5 cm, and then increased again to reach values >400 μM at 10 cm (Figure 3A). In the summer experiment, Fe_d concentrations above the detection limit were measured only in the upper 2.5 cm in all cores. In all summer irrigated cores, Fe_d concentrations were the highest in the samples closest to the SWI and reached concentrations of ~ 150 μM. In the non-irrigated cores, Fe_d concentrations reached maximum values of 50-100 μM (Figure 3E). In both seasons, Fe_d in the initial cores were lower than at the end of the experiments, with maximum values of ~100 μM in the winter and ~ 50 μM in the summer.

The winter experiment showed relatively constant SO_4^{2-} concentrations with depth in the initial and irrigated cores, averaging 26.3 ± 0.5 mM and 23.3 ± 0.9 mM, respectively (Figure 3B). Sulfate concentrations in the non-irrigated cores decreased slightly with depth, on average 1.9 mM lower at mid-depth in the cores and increase towards the bottom of the cores. Sulfate concentrations were also relatively constant in the initial and irrigated cores in the summer experiment with average concentrations of 23.6 ± 0.8 mM and 25.4 ± 0.7 mM, respectively (Figure 3F). SO_4^{2-} concentrations in the non-irrigated cores decreased with depth, on average 5.2 mM lower in the bottom sample than in the topmost sample. Porewater chloride concentrations were generally constant with depth (data not show).

Hydrogen sulfide (H_2S) concentrations were below detection limit in all samples from the winter experiment. In the non-irrigated cores of the summer experiment, hydrogen sulfide concentrations started to increase at 1.5-2.5 cm below the sediment surface and reached maximum values of 1000-1500 μM at ~6 cm before decreasing with depth. In the irrigated cores, H_2S was detected in the shallowest samples at ~0.5 cm depth and reached peak values of 400-500 μM at ~3.5 cm before decreasing with depth (Figure 3G).

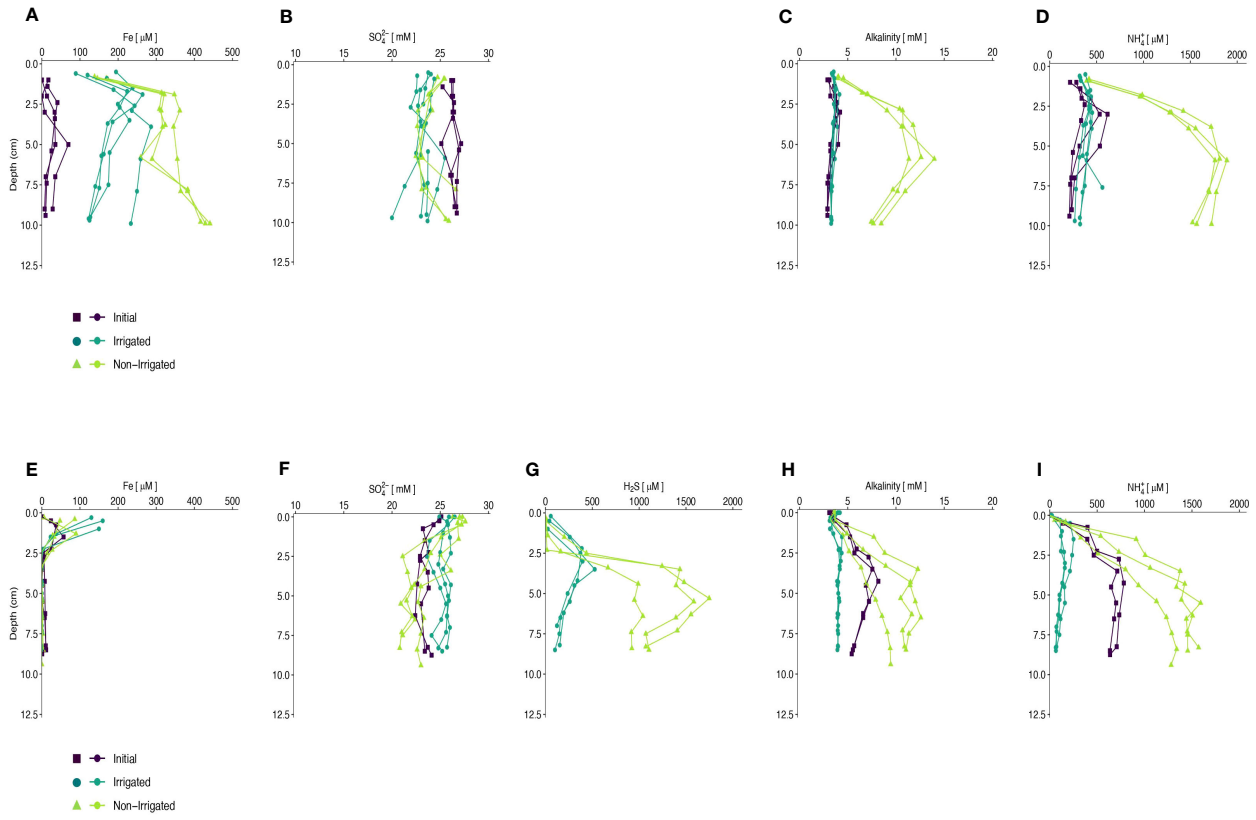

FIGURE 3
Porewater constituents (Fe, SO_4, H_2S, Alkalinity, and NH_4^+) plotted with depth (cm) in winter **(A–D)** and summer **(E–I)**. Initial core porewater values are depicted by purple squares, Non-Irrigated core porewater values are depicted by green circles, and Irrigated core porewater values are depicted by blue triangles.

Alkalinity concentrations in the initial and irrigated cores in the winter were relatively constant at depth with values ~5 mM. Alkalinity concentrations increased in the non-irrigated core to maximum values of 10-15 mM at ~6 cm depth and decreased below (Figure 3C). Alkalinity values in the summer initial cores increased with depth to a maximum of 8 mM at 4.5 cm, and then decreased below. In the non-irrigated cores, alkalinity values increased with depth to 7-12 mM at ~4.5 cm, and then remained constant with depth. The irrigated cores showed a slight decrease in TA in the top 0.5 cm, but then values remained constant at 5 mM (Figure 3H).

Concentrations of ammonium (NH_4^+) in the initial cores of the winter experiment increased steadily with depth in the top 3 cm and remained at a relatively constant value of ~550 µM for the remainder of the core. In the non-irrigated cores, NH_4^+ concentrations increased to maximum values of 2000 µM at ~6 cm, and then remained relatively constant with depth. In the irrigated cores, NH_4^+ increased in the top 2 cm to values ~500 µM before decreasing below (Figure 3D). The summer experiments showed similar profiles to the winter experiments, however maximum NH_4^+ values were different. In the initial cores the maximum NH_4^+ concentration was ~750 µM, in the non-irrigated cores the maximum value detected was 1000-1500 µM, and in the irrigated cores the maximum values were ~250 µM (Figure 3I).

The relative ratio of C:N estimated in the non-irrigated cores from linear regressions of porewater concentrations of alkalinity vs NH_4^+ (assuming that the non-irrigated treatment was a closed system with no differential diffusion and little NH_4^+ adsorption) was 5.1 in the winter and 5.6 in the summer (Supplemental S1).

3.1.2 Benthic iron flux

In the winter experiment, the Fe_d flux from irrigated sediments was greater than the flux out of the non-irrigated sediments (Figure 4A). After irrigation was initiated on Day 3, there was a sustained elevated flux of Fe_d on Days 3-5, averaging 217 ± 55 µmol m^{-2} d^{-1} for all 4 irrigated replicates during that time frame. There was no evidence of a decreased Fe_d flux with a timescale corresponding to porewater volume turnover due to bioirrigation (~ 4 d). The flux decreased steadily throughout the course of the experiment and reached an average of 37 ± 12 µmol m^{-2} d^{-1} by the final 2 days of the experiment. The flux out of the non-irrigated sediments was low throughout the course of the experiment, with estimated Fe_d fluxes ranging from 0 -14 µmol m^{-2} d^{-1}, though mostly below 8 µmol m^{-2} d^{-1}. Similarly, once irrigation began in the summer experiment on Day 2, Fe_d fluxes from the irrigated cores were always greater than from the non-irrigated cores (Figure 4B). There was an initial pulse of Fe on the day irrigation began, averaging 130 ± 61 µmol m^{-2} d^{-1} and values stabilized at 80 ± 42

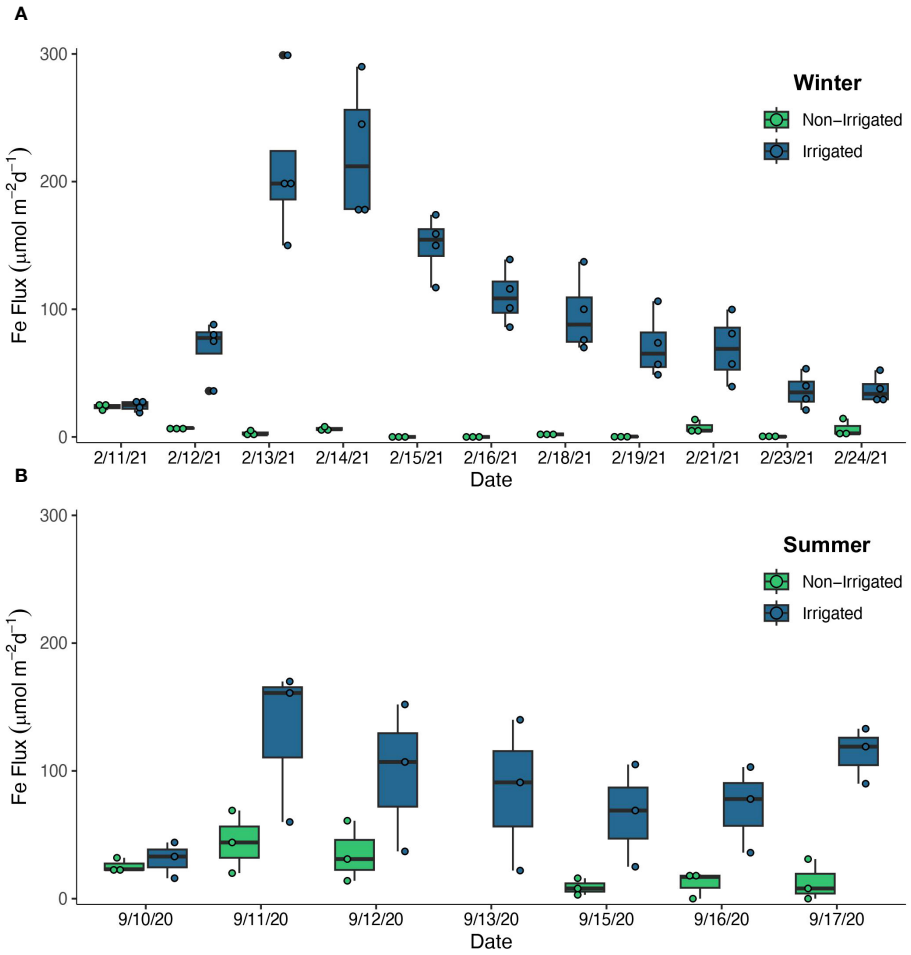

FIGURE 4
Fe accumulator Fe flux (μmol m^{-2} d^{-1}) estimates over the course of the winter experiment **(A)** and summer experiment **(B)**. Estimates from the Non-Irrigated cores are shown in green and estimates from the Irrigated cores are shown in blue. Vertical lines indicate the minimum and maximum values, the horizontal lines indicate the median value, and the boxes indicate the interquartile range. Non-irrigated treatments had 3 replicates per time point, and Irrigated treatments had 3 replicates (summer) or 4 replicates (winter) per time point.

μmol m^{-2} d^{-1} for all irrigated replicates for the remainder of the experiment. The fluxes from the non-irrigated core initially averaged 40 ± 22 μmol m^{-2} d^{-1} over the first three days, and then averaged 11 ± 10 μmol m^{-2} d^{-1} in the second half of the experiment.

3.1.3 Solid-phase composition

3.1.3.1 Iron contents

The initial core of the winter experiment had the greatest highly reactive Fe content (defined as the sum of Fe_{HCl}, $Fe_{Dith,}$ and Fe_{Pyrite} fractions) in the topmost cm, with a value of ~19.0 μmol Fe g^{-1} (Figure 5A), with residual reactive Fe-oxides ($Fe(III)_{HCl}$ and Fe_{Dith}) having a value ~9 μmol Fe g^{-1}. Between 2 and 12 cm, the residual reactive Fe content remained relatively constant and averaged at 3.8 ± 0.5 μmol Fe g^{-1}, though total reactive Fe (driven by differences in Fe_{pyrite}) was lower mid-depth, and higher at the bottom of the core. At the end of the experiment, the irrigated core was characterized by a substantial enrichment of highly reactive Fe in the top 0.2 cm with a value ~ 31 μmol Fe g^{-1} (Figure 5C). There was also a slight surface enrichment (~15 μmol Fe g^{-1}) in the non-irrigated core relative to the deeper sediment layers, however, its Fe content was less than the value observed in the initial core (Figure 5B). Residual reactive Fe-oxide contents in the remainder of the cores from both treatments remained constant with depth with an average value of 3.2 ± 0.4 μmol Fe g^{-1} for the non-irrigated core (excluding the surface scrape sample) and 3.1 ± 0.4 μmol Fe g^{-1} for the irrigated core (excluding the surface scrape sample). In both treatments, total reactive Fe followed a similar trend to the initial core, with lower concentrations mid-depth, and higher concentrations at the bottom of the core. In the irrigated treatment, the Fe-oxide content within the irrigated pocket was greater than in the surrounding bulk sediment with 4.7 ± 0.1 μmol Fe g^{-1} from 10-14 cm sediment depth compared to 2.8 ± 0.4 μmol Fe g^{-1}, however, the bulk sediment made up the difference with greater $Fe_{HCl}(II)$ contents. The Fe-oxide inventory of the initial core was estimated to be ~84 μmol Fe cm^{-2} (summation of the individual interval inventories, e.q. 1), while estimates for the non-irrigated and irrigated cores were ~66 μmol Fe cm^{-2} and ~70 μmol Fe cm^{-2}, respectively. Relative contributions of $Fe_{HCl}(II)$, $Fe_{HCl}(III)$, $Fe_{Dith,}$

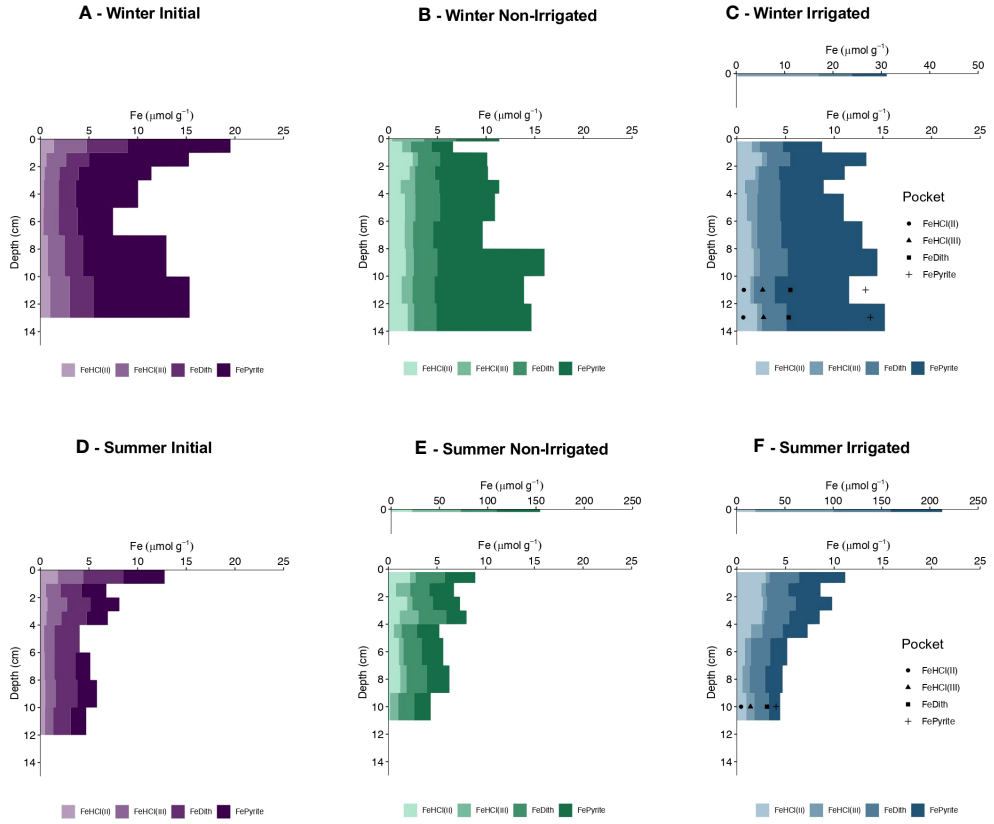

FIGURE 5
Highly reactive Fe content (μmol g^{-1}) with depth (cm) in one of the winter cores **(A–C)** and in one of the summer cores **(D–F)**. Shown are HCl-extractable Fe(II) and Fe(III), labeled Fe_{HCl}(II) and Fe_{HCl}(III) respectively, and dithionite- extractable Fe, labeled Fe_{Dith} and pyrite Fe as determined stoichiometrically from chromium reducible sulfur contents, labeled Fe_{pyrite}. Initial core values are shown in shades of purple, Non-Irrigated core values are shown in shades of green, and Irrigated core values are shown in shades of blue. Values of reactive Fe within the irrigated pocket are depicted by shapes (Fe_{HCl}(II) = circle, Fe_{HCl}(III) = square, Fe_{Dith} = triangle, Fe_{pyrite} = plus) displayed cumulatively in the middle of the depth fraction sampled. Values from the surface scraping for the Winter Irrigated core **(C)**, Summer Non-Irrrigated **(E)**, and Summer Irrigated **(F)** were plotted on a larger scale above their respective main figure panels.

Fe_{Pyrite} to the highly reactive pool were 14%, 7%, 17%,and 59%, respectively, for the non-irrigated core and 12%, 7%, 19% and 57% for the irrigated core.

The initial core of the summer experiment displayed the greatest highly reactive Fe content in the top 1 cm, with a value of ~12.8 μmol Fe g^{-1} (Figure 5D), with a residual reactive Fe-oxide content of 6.8 μmol Fe g^{-1}. Below 1 cm, total reactive Fe decreased between 1-6 cm and decreased further between 6-11 cm. The Fe-oxide content averaged 4.0 ± 0.4 μmol Fe g^{-1} between 1-6 cm and then slightly decreased to average values of 3.0 ± 0.3 μmol Fe g^{-1} between 6-11 cm sediment depth. At the end of the experiment, the cores from the non-irrigated and irrigated treatments showed large enrichments of highly reactive Fe in the top 0.2 cm, reaching values of ~151 and ~210 μmol Fe g^{-1}, respectively (Figures 5E, F). Cores from both treatments also had similar downcore trends as the initial core with a decrease in total reactive Fe and in Fe-oxides with depth. In the non-irrigated core, the Fe-oxide content in the upper 4 cm (excluding the surface most sample) averaged 3.1 ± 0.9 μmol Fe g^{-1}, and at 4-11 cm sediment depth averaged 2.4 ± 0.2 μmol Fe g^{-1}. In the irrigated core, the Fe-oxide content in the upper 5 cm (excluding the surface most sample) averaged 3.1 ± 0.3 μmol Fe g^{-1} and averaged 2.4 ± 0.2 μmol Fe g^{-1} at 5-11 cm sediment depth. In the irrigated treatment, the Fe-oxide content within the irrigated pocket was slightly higher (~3 μmol Fe g^{-1}) than the surrounding bulk sediment, however, the surrounding bulk sediment had greater Fe_{HCl}(II) contents (Figure 5F). The Fe-oxide inventory of the initial core was estimated to be ~77 μmol Fe cm^{-2}, while estimates for the non-irrigated and irrigated cores were ~ 70 μmol Fe cm^{-2} and ~70 μmol Fe cm^{-2}. Relative contributions of Fe_{HCl}(II), Fe_{HCl}(III), Fe_{Dith}, Fe_{Pyrite} to the highly reactive pool were 14%, 18%, 32% and 36%, respectively, for the non-irrigated core and 20%, 16%, 31%, and 33% for the irrigated core.

3.1.3.2 Iron monosulfide and pyrite content

In the cores from the winter experiment no acid volatile sulfide (AVS) was detected. The initial core displayed the highest chromium reducible sulfur (CRS) content in the surface 2 cm with an average value of 20.8 ± 0.4 μmol S g^{-1}. Below this depth CRS values decreased to 7.2 μmol S g^{-1} at 5-7 cm before increasing again to 19.7 μmol S g^{-1} in the deepest horizon of the core (Figure 6A). The non-irrigated core showed lower CRS values in the top 2 cm than in the initial core with an average value of 7.7 μmol S g^{-1} (Figure 6B). Below, CRS contents increased with depth,

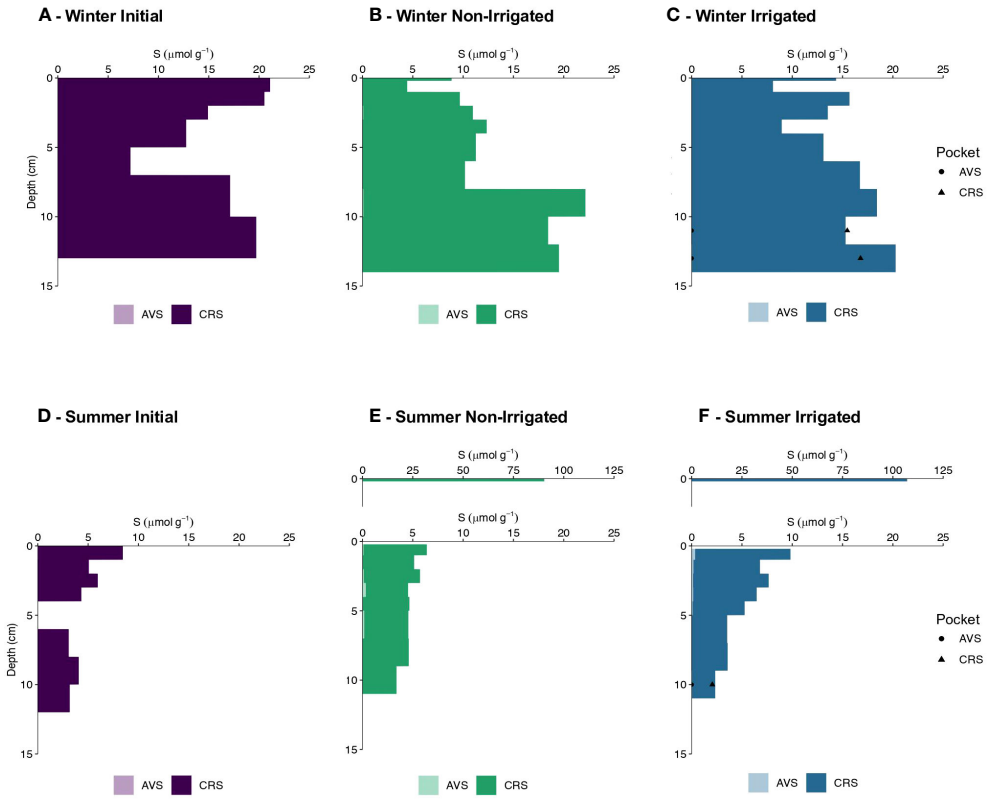

FIGURE 6
Acid volatile sulfide (AVS) content (μmol g^{-1}) and chromium reducible sulfur (CRS) content (μmol g^{-1}) with depth (cm) in winter **(A–C)** and summer **(D–F)**. Initial core values are shown in shades of purple, Non-Irrigated core values are shown in shades of green, and Irrigated core values are shown in shades of blue.

averaging 20 ± 1.9 μmol S g^{-1} at the bottom of the core. CRS content in the irrigated core was variable with no clear vertical trend, averaging 14.4 ± 4.0 μmol S g^{-1} (Figure 6C). The upper section of the irrigated pocket (10-12 cm) had similar CRS contents as the surrounding bulk sediment, however, the deeper section of the irrigated pocket (12-14 cm) had lower CRS content to the surrounding bulk sediment (6C). The estimated inventories of CRS for the non-irrigated and irrigated cores were 225 and 249 μmol S cm^{-2}, respectively.

In the summer experiment, there was no AVS in the initial core, and less than 0.35 μmol S g^{-1} in the non-irrigated and irrigated cores. In the non-irrigated core, measured values ranged from 0.03-0.33 μmol S g^{-1}, with the maximum value determined between 3-4 cm depth (Figure 6E). The irrigated core showed a similar range of AVS concentrations with values of 0.04-0.34 μmol S g^{-1} and the maximum value detected at 0.2-1 cm sediment depth (Figure 6F). The initial core of the summer experiment displayed the highest CRS content in the top 1 cm with a value of 8.4 μmol S g^{-1}. CRS values between 1-4 cm depth averaged 5.0 ± 0.9 μmol S g^{-1} and averaged 3.4 ± 0.5 μmol S g^{-1} in the bottom layer (Figure 6D). Both non-irrigated and irrigated cores were characterized by surface layer enrichments in CRS, with maximum values of 90.2 and 107.1 μmol S g^{-1} (Figures 6E, F), respectively. There was no trend in CRS content with depth observed in the remainder of the non-irrigated core with average CRS values of 4.4 ± 0.7 μmol S g^{-1}. In contrast, the irrigated core displayed a distinct trend with depth. Below the top 1 cm, CRS concentrations decreased from 6.3 μmol S g^{-1} between 1-2 cm to 2.3 μmol S g^{-1} between 9-11 cm (Figure 6F). There was no difference between the CRS content in the irrigated pocket and the surrounding bulk sediment (6F). Although the distribution throughout the cores varied, the estimated inventories of CRS were very similar in the non-irrigated and irrigated cores with values of 91 and 94 μmol S cm^{-2}, respectively.

3.1.3.3 Total organic carbon

Total organic carbon (TOC) content in the winter initial core was the greatest in the top 1 cm with ~0.39 wt. % TOC, and then decreased with depth (Figure 7). TOC remained relatively constant with depth at ~0.15 wt. % in the bottom 10 cm of the core. TOC in the summer initial core was also the greatest in the top 1 cm with a value of 0.22 wt. % TOC, and then decreased with depth (Figure 7). TOC remained relatively constant with depth with average values of ~0.09 wt. % in the bottom 7 cm of the core.

3.2 Field monitoring of reactive Fe-oxide inventories

Reactive Fe-oxide inventories in the top 15 cm of the sediment at the field site varied over the course of the year (Supplemental

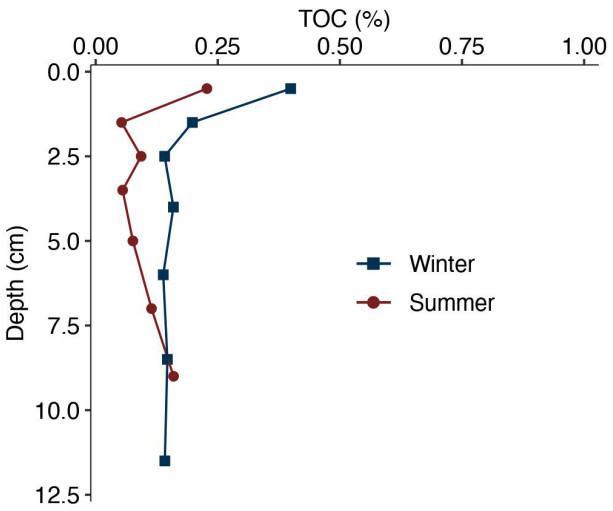

FIGURE 7
Total organic carbon (TOC) content (wt. %) with depth (cm) in winter and summer initial cores. Winter values are shown by the blue squares, and summer values are show by the red circles.

Figures S5–S8). Inventories at the onset of monitoring in July were ~75 μmol Fe cm^{-2} in the lower intertidal and ~60 μmol Fe cm^{-2} in the higher intertidal sites. The inventories decreased during September to December to ~60 μmol Fe cm^{-2} in the low intertidal and ~30 μmol Fe cm^{-2} in the high intertidal. Inventories were higher in February through April and peaked in April at ~100 μmol Fe cm^{-2} in the low intertidal and ~60 μmol Fe cm^{-2} in the high intertidal sites. In all months at both sites, the reactive Fe inventories were higher in the lower intertidal which was the site with high densities of *C. torquata* (Figure 8).

4 Discussion

4.1 Biogeochemical processes in permeable sandy sediments in winter and summer

Our experiments were designed to accurately simulate conditions imposed by bioirrigators in permeable sandy sediments. They allowed us to study the biogeochemical processes and bioirrigation-induced Fe_d fluxes from sandy sediments in different seasons and to specifically isolate the effects of seasonality and bioadvective transport.

4.1.1 Biogeochemical iron cycling and release in permeable sandy sediments during winter

Porewater profiles were characterized by elevated Fe_d concentrations at all depths in both the irrigated and the non-irrigated cores of the winter experiment, reaching values >400 μM in the deepest sections of the non-irrigated cores (Figure 3A). The accumulated Fe was likely sourced from multiple pathways as the product of both initial and secondary reactions linked to the oxidation of organic matter. Dissolved Fe is released directly during dissimilatory iron reduction (DIR) coupled to the oxidation of organic matter (Canfield, 1989; Lovley, 1997) and through the reduction of Fe-oxides by H_2S (Millero, 1991; Poulton et al., 2004), in which H_2S is also a product of organic matter oxidation via

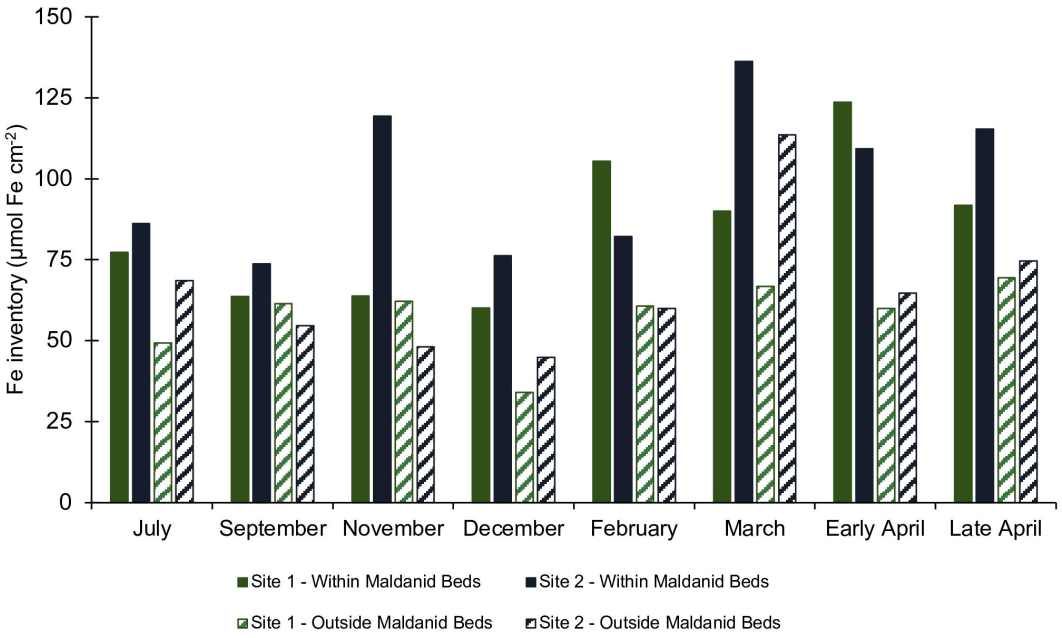

FIGURE 8
Reactive Fe depth integrated inventories in the top 15 cm (Fe_{HCl}(II) + Fe_{HCl}(III) + Fe_{Dith}) of sediment cores collected at field monitoring sites #1 (green) and site #2 (blue) from July 2021 through late April 2022. Solid color bars represent cores from within the densely populated maldanid bed, and stripes represent cores from outside the maldanid bed.

sulfate reduction. Additional products of organic matter oxidation, ammonium (NH_4^+) and alkalinity, also increased in the porewater (Figures 3C, D) supporting the assumption of organic matter oxidation-driven Fe release.

Small but discernable decreases in sulfate concentration with depth provide further evidence for the occurrence of sulfate reduction in the winter experiment (Figure 3B). Since H_2S did not accumulate in porewater, and there was no build-up of AVS (Fe-monosulfide) or CRS (pyrite, elemental sulfur) at any depth, H_2S was likely being rapidly reoxidized by Fe-oxides, releasing additional Fe_d into the porewater (Pyzik and Sommer, 1981), and resupplying sulfate to the porewater pool. However, the increase of the Fe(II) fraction in the HCl-extractable solid phase in the final non-irrigated and irrigated cores compared to the initial cores, may suggest minor Fe-monosulfide formation that was below the analytical detection limit of the AVS method (0.02 μmol g^{-1}), however this cannot account for the full magnitude of the increase in the Fe(II) fraction. It is likely that the increase of solid-phase Fe may also reflect Fe-carbonate formation as the porewater was calculated to be saturated with respect to siderite or it could possibly be Fe^{2+} adsorbed to the remaining Fe-oxide pools. In the winter experiment, the residual reactive ($Fe(III)_{HCl}$ and Fe_{Dith}) Fe-oxide pools appear to be sufficiently large to effectively reoxidize and sequester any formed H_2S, preventing any significant accumulation of H_2S in the porewater. By the end of the experiment, CRS contents in the upper half of the sediment column in the irrigated and non-irrigated winter cores were lower than in the initial cores (Figures 6A-C), indicating that pyrite oxidation may have additionally taken place over the course of the experiment. This could also have provided an additional pathway for Fe_d formation (Aller, 1980).

There was an increase of Fe_d in the porewater below 6.5 cm in the non-irrigated cores, possibly related to lower concentrations and less labile organic matter in winter, which would have led to a decrease in sulfate reduction rates (Westrich and Berner, 1984) driving less scavenging of Fe_d by reaction with H_2S to form Fe-monosulfides, thus allowing for greater buildup of Fe_d in the porewater at depth. This inference is supported by lower sulfate concentrations at mid-depth, which indicated elevated consumption of sulfate via sulfate reduction compared to deeper sections which had higher sulfate concentrations (Figure 3B). Decreasing total carbon remineralization rates below 6.5 cm are consistent with NH_4^+ and alkalinity concentration declines below this depth compared to the zone above (Figures 3C, D), providing evidence for lower production rates of these constituents in the deepest sediment zone.

4.1.2 Biogeochemical iron cycling and release in permeable sandy sediments during summer

In the summer experiment, Fe_d in the porewater was limited to the upper 2.5 cm of the sediment in both the irrigated and non-irrigated cores. The Fe_d was also likely produced during organic carbon remineralization, released both during DIR (Canfield, 1989) and the reduction of Fe-oxides by H_2S (Millero, 1991; Poulton et al., 2004). Elevated organic carbon remineralization rates were evidenced by the significant accumulation of both NH_4^+ and alkalinity with depth in the experimental cores compared to the initial cores. In the non-irrigated cores, the decrease of porewater sulfate concentration with depth and increase of H_2S directly below 2.5 cm suggest elevated rates of sulfate reduction (Berner, 1978). The presence of free H_2S in the porewater likely was the result of the decrease in the reactive Fe-oxide pool below the surface (Figure 5E). The enrichment of CRS at the surface in summer sediments is evidence for the reaction between H_2S and Fe_d and Fe-oxides and could represent elemental sulfur formed during the reoxidation of sulfide by Fe-oxides, and pyrite formed near the SWI (Berner, 1970; Pyzik and Sommer, 1981; Liu et al., 2020).

4.1.3 Differences in biogeochemical iron-sulfur cycling between summer and winter

In the sandy sediments we studied, Fe-S cycling dynamics varied seasonally. These differences resulted in large variations in both the porewater Fe_d and H_2S concentrations, and in the solid phase composition of the sediment in the experimental cores from the summer and the winter. The differences between the seasons may be explained by 1) differences in solid-phase Fe content and distribution, and 2) variations in total organic carbon mineralization rates as a result of differences in organic carbon concentrations and lability as well as temperature differences between summer and winter. Differences in the pumping frequency and depth of water injection by bioirrigators likely further contributed to the seasonal differences in geochemical parameters (Dwyer et al., in review).

Reactive Fe-oxide (HCl- and dithionite extractable) inventories were similar in summer and winter cores. However, relative distribution between the different pools and distribution with depth showed seasonal variations, likely contributing to the geochemical variability observed in the experiments during the two seasons. In the winter, the initial cores had larger contents of easily reducible $Fe(III)_{ox}$ (determined by HCl extraction) at all depths than in the summer cores. The easily reducible $Fe(III)_{ox}$ was also more evenly distributed in the winter than in the summer, which had elevated concentrations in the top 4 cm, and lower concentrations in deeper layers (Figure 4). These Fe-oxides, most likely comprised of ferrihydrite and lepidocrocite, can most readily undergo diagenetic processes, including dissimilatory iron reduction (DIR) and reaction with H_2S (Lovley and Phillips, 1986; Canfield, 1989). The higher easily reducible $Fe(III)_{ox}$ content in winter likely supported greater rates of DIR and enhanced scavenging and reoxidation rates of H_2S produced by sulfate reduction (Michaud et al., 2020). As a product of both processes, during the winter there was a much larger pool of Fe_d in the porewater. The smaller $Fe(III)_{ox}$ contents in the summer, especially at depth, were likely a controlling factor allowing for less DIR and reoxidation of H_2S, contributing to the high H_2S concentrations at depth (Figure 4).

Differences in carbon remineralization rates and pathways in summer and winter may have played a role in influencing the observed variations in geochemical conditions, including porewater characteristics. Typically, lower organic matter concentration and a

decrease in lability of the organic matter, which generally occurs in the winter when primary production is lower due to light limitation and thus limited transport of fresh organic matter to the sediments, lead to lower overall carbon remineralization rates (Jorgensen, 1978; Westrich and Berner, 1984; Burdige, 1991; Green et al., 2004). Lower temperatures in winter have also been shown to slow down microbial processes in the sediment, therefore lowering the rates of carbon remineralization processes including DIR and sulfate reduction (Klump and Martens, 1989; Pomeroy and Wiebe, 2001; Koretsky et al., 2003; Gudasz et al., 2010). However, total organic carbon (TOC) content in the initial cores showed similar starting TOC contents in both summer and winter. Additionally, when we estimated the NH_4^+ production rates for both experiments by dividing the end of experiment NH_4^+ inventory by the length of the experiment, we found similar production rates for both summer and winter. Intriguingly, the estimated production was ~ 64 µmol d^{-1} in the winter and ~63 µmol d^{-1} in the summer, indicating that organic carbon remineralization rates were quite similar in both seasons. However, it is possible that given typically higher total carbon remineralization rates during the summer, the labile organic carbon pool was actually exhausted after a few days during the course of the experiment, limiting NH_4^+ production and apparent carbon remineralization rates thereafter. This is especially possible considering permeable sands tend to have relatively low standing stocks of labile organic carbon (Jickells and Rae, 2005) and sustained inputs via particle advection typical for permeable sands (Huettel et al., 1996; D'Andrea et al., 2002; D'Andrea et al., 2004) were not simulated in our incubation experiments.

We found that in the summer, there was a more pronounced decrease in sulfate concentration with all depths than in the winter, consistent with higher sulfate reduction rates. The depth integrated loss of SO_4 inventory in the top 7.5 cm of the non-irrigated cores was calculated and used to estimate an average net depth integrated SO_4 reduction rate of ~12 mmol m^{-2} d^{-1} over the course of the 11-day summer experiment, which is similar to rates reported (0.54-39.4 mmol m^{-2} $d^{-1)}$ from permeable sands in Sylt, Germany in summer (Seibert et al., 2019). In winter, sulfate reduction rates were estimated to be ~3 mmol m^{-2} d^{-1} in the upper 7.5 cm, below which, sulfate concentrations increased, indicating even lower rates. Most H_2S produced in winter was reoxidized, likely by Fe-oxides, and therefore, there was no H_2S accumulation within the porewater, as opposed to high H_2S concentrations in the summer. It is possible that the apparent sulfate reduction rate in winter may be obscured by the reoxidation of sulfide back to SO_4, however this would not explain the 4-fold higher sulfate reduction rate in summer compared to winter. A seasonal decrease in sulfate reduction rate would generally suggest that organic carbon availability, especially at depth, may be different between the seasons. However, starting TOC content were similar in both summer and winter, and overall estimated carbon remineralization rates based on NH_4^+ production were also similar. This may indicate that there is instead a seasonal shift in the contribution of different carbon remineralization pathways to total organic carbon remineralization, with a larger contribution of sulfate reduction in the summer and higher contribution of dissimilatory iron reduction in the winter (Koretsky et al., 2003). This could be due to lower temperatures (Koretsky et al., 2003), the greater availability of $Fe(III)_{ox}$ allowing for more DIR, and perhaps a resulting shift in bacterial assemblage towards more Fe-reducing bacteria in the winter (Koretsky et al., 2003). These results suggest that the availability of $Fe(III)_{ox}$ and the temperature play important roles in driving seasonal differences in carbon remineralization pathways.

Though the total CRS inventory was higher in the winter, this was likely not primarily due to new pyrite formation, as this process would have been limited by H_2S production. The higher CRS in winter was more likely a remnant of the observed summer Fe-S dynamics with rapid pyrite formation at the surface. We hypothesize that in the summer the very frequent pumping activity of bioirrigators drives efficient H_2S reoxidation (se section 4.2), while in the fall the pumping activity of the benthic macrofauna likely decreases resulting in enhanced pyrite formation reflected in the elevated CRS values observed for the winter cores. As sulfate reduction rates in the late fall/winter decrease, the porewater switches from being H_2S- to being Fe_d -dominated and little additional pyrite is produced. When pumping frequencies by bioirrigators increase again in the spring, the enhanced introduction of oxygen into the sediment likely results in the efficient reoxidation of the winter CRS pool to summer values. CRS was potentially a source of porewater Fe_d via pyrite oxidation as opposed to a sink in the sediments during the summer, which may be supported by the observed decrease in CRS in the upper 5 cm in the end of experiment winter cores (6B, C) relative to the initial core (6A). Pyrite oxidation during the winter may also have contributed to the larger Fe-oxide inventory, as Fe-oxides are the terminal product of pyrite oxidation (Luther et al., 1982; Hu et al., 2006).

4.2 Effect of bioirrigation on sedimentary biogeochemical process and Fe fluxes

In these experiments we employed bioirrigation mimics that injected fully oxic overlying water into the sediment at depth to investigate the effects of burrow ventilation and the associated advective porewater transport on biogeochemical processes and benthic Fe fluxes. Non-irrigated cores allowed us to study iron cycling and related processes in permeable sediments in the absence of advective transport.

4.2.1 The effect of oxygen transport into the sediment on geochemical properties

A major component of bioirrigation in sediments can be the injection of oxygen-rich water into anoxic sediments at depth (Volkenborn et al., 2019). Irrigation by macrofauna increases the total sediment O_2 uptake (Forster and Graf, 1995), and creates oxic zones around burrows at depth in otherwise anoxic sediments (Aller, 1982; Kristensen and Kostka, 2005), which both have implications for carbon remineralization and related geochemical processes within the sediment.

While the transport of oxygen into the sediment at depth by the irrigation mimic did not appear to have significant effects on bulk solid-phase sediment in the timeframe of our experiments, there

were clear geochemical impacts in the sediment directly surrounding the area of water injection at depth. This was observed visually with a light-colored sphere of more oxidized sediment around the injection port (Supplemental S4) but also resulted in differences in the solid-phase reactive Fe and CRS contents in both winter and summer experiments (Figures 5, 7). The sediment at depth had a greater percentage of Fe_{HCl}(III) than Fe_{HCl}(II) (Supplemental S3) within the injection pocket than in the surrounding bulk sediment. This difference suggests reoxidation of reduced Fe (Figure 5) to Fe-oxides. Similarly, the CRS content was lower in the injection pocket than in the surrounding bulk sediment, likely due to pyrite oxidation.

The injection of oxic water at depth was also responsible for the reoxidation of reduced porewater constituents, particularly near the point of injection, consistent with other studies (Huettel, 1990; Quintana et al., 2015; van de Velde and Meysman, 2016). Given the distinct differences in Fe-S-dynamics between the summer and winter, this effect was most apparent in the Fe_d concentration profiles of the winter irrigated cores (Figure 3A), and the H_2S profiles of the summer irrigated cores (Figure 3G). In both cases, concentration peaks occurred at ~2.5 cm depth, below which concentrations decreased. In contrast, Fe_d concentrations in the non-irrigated cores in winter and H_2S concentrations in summer increased with depth, suggesting that there was continued production of these porewater constituents in the sediments at depth, but in the irrigated cores reoxidation led to their partial removal from the porewater. The observed reoxidation of reduced Fe constituents, like Fe_{HCl}(II), CRS, and Fe_d, to Fe_{HCl}(III) likely supported a relative higher contribution to DIR in the winter irrigated cores compared to the non-irrigated cores.

4.2.2 Bioadvective transport and benthic Fe_d flux

The advective transport induced by the injection of water at depth had a significant impact on the biogeochemical properties of the sediment, and ultimately controlled the magnitudes of the fluxes of remineralization products, including Fe_d, NH_4^+, and alkalinity, into the overlying water. In both seasons, the irrigated cores had shallower peaks and overall, much lower concentrations of a range of porewater constituents, including Fe_d, NH_4^+, and alkalinity than non-irrigated cores. While the lower concentrations were also partially the result of oxidation at depth, the key driver of these profiles was likely advective transport. These observations are consistent with previous findings that water flow through permeable sediments induced by burrow ventilation leads to efficient porewater flushing (Huettel, 1990; Banta et al., 1999; Volkenborn et al., 2007b). This mechanism is particularly effective in high permeability sands, such as the sediments used in our experiments, where small pressure gradients created by infaunal organisms can cause porewater transport over distances of tens of cm (Meysman et al., 2006; Wethey et al., 2008).

The upward transport of porewater constituents was expressed by the relative location of concentration peaks. In both seasons, maximum porewater NH_4^+ and alkalinity concentrations in the irrigated cores were located closer to the SWI than in the non-irrigated cores, in some cases offset by more than ~2 cm (Figures 3D, I). In the summer, H_2S appeared closer to the SWI interface in the irrigated cores, indicating a compression of the suboxic zone. All irrigated cores also had higher concentrations of Fe_d in the upper 2.5 cm compared to the non-irrigated cores, further highlighting the transport of reduced constituents towards the SWI —and indicating the enhanced potential of Fe_d transport across the SWI due to bioadvection.

As a result of the upward transport of reduced constituents (including Fe_d) and narrowing of the oxic zone near the SWI, a greater precipitation of Fe-minerals at the surface in the irrigated sediments was also observed. The surface scrape samples from the irrigated cores were more enriched in solid-phase reactive Fe-oxides and CRS than in the non-irrigated cores in both summer and winter (Figures 5, 7). During both seasons, the upward porewater advection transported more Fe_d towards the SWI and into a narrow oxic zone, where Fe precipitated as Fe-oxides in a confined layer at the surface. The Fe-oxide content may have been further enriched by Fe_d that was quickly reoxidized and scavenged within the overlying water and then redeposited on the sediment surface. In the summer, the advective upward transport of both Fe_d and H_2S likely created a surface reaction zone where rapid Fe-S cycling involved multiple reaction pathways. In the upper parts of the surface zone, Fe_d and H_2S were rapidly oxidized by oxygen (and in the case of H_2S, also by Fe(III)oxides) leading to the formation of new Fe(III) oxide phases and intermediate sulfur species and sulfate, respectively (Luther, 1987; Zopfi et al., 2004). At the interface where both reactants were present at elevated concentrations, their reaction also led to the formation of iron monosulfide (AVS), which appears to have been quickly further transformed to elemental sulfur and pyrite as indicated by the absence of an AVS peak but elevated CRS concentrations at the sediment surface (Rickard and Luther, 2007). The cryptic sulfur cycling in this zone also likely included the interaction of elemental sulfur with sulfide to form polysulfides which could then have taken part in reactions with AVS to form pyrite (Luther, 1991; Schoonen and Barnes, 1991; Wilkin and Barnes, 1996; Rickard and Luther, 2007).

While a fraction of the Fe_d that was advected to the surface sediment was reoxidized by oxygen, our Fe flux data indicate that a significant proportion was also transported into the overlying water column. Fe_d flux estimates from the irrigated cores in summer and winter were significantly higher than those from the non-irrigated cores, reaching maximum fluxes of >150 μmol m^{-2} d^{-1} in summer and >200 μmol m^{-2} d^{-1} in winter (Figure 4). These results suggest that permeable sands have the potential to release large Fe_d fluxes under fully oxic overlying water conditions with active bioirrigation present. They also suggest that the bioadvection induced by irrigation or physical advection by waves/currents can be an important driver of benthic Fe_d fluxes from permeable sands. This impact can be highlighted by the comparatively low Fe_d fluxes from the non-irrigated sediments even with high Fe_d production and porewater inventories (Figures 3A, E). Assuming similar Fe_d production rates between the non-irrigated and irrigated cores in the winter, ~10% of Fe_d inventory was released from the irrigated cores, whereas <0.05% was released from the non-irrigated cores over the course of 12 days. It should also be emphasized that even though depth integrated porewater inventories were relatively

low in the summer compared to the winter, 0.5 mmol m^{-2} and 11.4 mmol m^{-2} in the non-irrigated cores, respectively, fluxes remained high from the irrigated cores throughout the experiment. This suggests that low porewater inventories in permeable sediments can be an expression of high fluxes in a well-flushed bioadvective systems, as seen in the summer experiment, or other physically advective systems rather than imply a low benthic Fe_d flux. Sustaining such high fluxes, however, would depend on the replenishment of reactive Fe and labile C_{org} by particle filtration and capture into the seabed. While this mechanism is limited in the laboratory incubation experiments, it was apparent in field inventories (see 4.2.3).

The Fe-oxide enrichment resulting from the advective transport of Fe_d into the surface layers of the irrigated cores likely helped sustain the higher fluxes from irrigated sediments. The redistribution of Fe to the surface resulted in the dynamic Fe-S cycling occurring closer to SWI than in the non-irrigated cores, which supported the release of some Fe_d into the porewater. The Fe_d could have then been more quickly transported out of the sediments during active irrigation, given the shorter distance between the reaction zone and the SWI, and therefore was less likely to participate in secondary reactions that retained Fe_d in the sediments.

While porewater Fe_d concentrations were higher in the winter than in the summer experiments, they did not correlate to correspondingly higher fluxes in either the irrigated or the non-irrigated cores. There was 3-5-fold higher porewater Fe_d inventory in the winter, but similar magnitude fluxes as in the summer from the irrigated cores, and the magnitude of summer fluxes from the non-irrigated cores was about two times higher than winter fluxes. This can be explained by a more effective "oxic lid" in the winter due to higher oxygen solubility at lower temperatures, allowing for deeper oxygen penetration into the sediments and reoxidation of Fe_d at the surface. Nearly 100% of the reactive solid-phase Fe in the surface was Fe-oxide [little $Fe_{HCl}(II)$] in the winter, demonstrating efficient reoxidation of Fe. The efficient reoxidation of Fe is also supported by recent work suggesting that longer pumping intervals by bioirrigators and lower carbon remineralization rates in the winter may provide more stable oxygen presence in the sediments, with less frequent switches between anoxic and oxic conditions than in the summer (Dwyer et al., in review), enhancing retention of available Fe_d in the sediments.

4.2.3 Effect of bioirrigation on Fe inventories in the field

Differences in reactive Fe concentration and distribution patterns that were observed between maldanid bed and non-bed sites in almost all months can also be attributed to the effect of bioirrigation and particle reworking on sedimentary Fe-S dynamics and to the interactions of deposits with overlying water suspended particles. The sample locations within the densely populated maldanid beds (1000-3000 individuals m^{-2}, Dwyer personal communication) had up to 30-50% larger solid-phase reactive Fe inventories (HCl and dithionite extractable Fe) than the sites outside the maldanid bed (Figure 8). All sites showed a regular seasonal inventory pattern of relatively higher inventories during late winter and early spring compared to summer and fall. Thus, the inventory patterns demonstrate that the intertidal regions accumulate and lose reactive Fe periodically. The dense maldanid beds clearly follow this overall pattern and further augment it, including the enhanced recapture of reactive Fe from the water column relative to other regions of the intertidal with lower infaunal abundances.

Particle size also appears to play a role in the seasonal differences in Fe inventories, with more fine-grained particles observed during microscopic analysis of the dry sediments in the months and depth intervals with elevated reactive Fe, particularly in the winter and early spring. This observation implies that the activities of maldanids can enhance the capture of small particles from the water column. It is well known that *C. torquata* preferentially select finer-grained particles at depth and redistribute them vertically within the sediment and into their feeding pockets, producing biogenic graded bedding and heterogeneity (Mangum, 1964; Rhoads, 1967; Wendelboe et al., 2013). Our data imply that bioirrigation and particle reworking by maldanids also results in a flux of fine particles from the water column into the deposits, presumably advected into the sediment during bioirrigation and also entrained during the deposition of fecal material at the sediment-water interface.

As shown in our experiments, bioirrigation enhances escape of Fe_d from these sands, much of which is reprecipitated as colloids and scavenged by small particles in the water column (or our Fed accumulators in the lab). Bioirrigation also results in the redistribution of reactive Fe internally within deposits. One expression of Fe redistribution in the field, for example, is that maldanid tubes within the densely populated area typically had rust-colored linings as a result of the oxidation and precipitation of Fe_d along burrow walls. This redistribution is unlikely to alter inventories *per se*. Thus, there appears to be an interplay of enhanced net Fe_d loss from bioirrigated deposits, reprecipitation of refluxes Fe_d on particles in the water column, and the recapture of small particles enriched in diagenetically remobilized Fe that results in overall enhanced reactive Fe inventories in the areas of high maldanid abundance. The overall impact of the activities of the maldanids is to intensify the recycling-refluxing of Fe between the sediment and overlying water in this sandy system.

4.3 Experimental considerations

By using bioirrigation mimics, we were able to successfully isolate bioadvection and evaluate its effect on Fe_d fluxes. Mimics, such as those used in these experiments have been shown to realistically simulate biogeochemical impacts on sediment, and to accurately replicate the oxic pocket formed by the injection of oxygen at depth and the advection of porewater out of the sediments (Meysman et al., 2006; Na et al., 2008; Matsui et al., 2011). Bioirrigation can be highly variable across species and locations (Kristensen et al., 2012; Volkenborn et al., 2012), and vary seasonally (Martin and Sayles, 1987; Schlüter et al., 2000). Our model organism, *C. torquata*, has been shown to have higher pumping frequency with shorter resting intervals in the

summertime and less frequent, but longer, pumping events in the winter (Dwyer et al., in review). We were able to capture the essence of this variability in our experiment by adjusting the time and frequency of injection.

Our closed system experimental set up, however, excluded other important components of bioturbation and other pressure driven advective flows characteristic of permeable sediments, including those caused by waves, currents and tidal forcings (Santos et al., 2012). These additional pressure driven advective components could also influence benthic Fe_d release by altering redox conditions at depth and by altering the flow path of water through sediments. The closed system also prevented the resupply of labile organic C and reducible $Fe(III)_{ox}$ at depth (Huettel et al., 1996; Huettel and Rusch, 2000; de Beer et al., 2005). Given the lengths of our experiments (~ 2 weeks), the labile C content was likely sufficient to approximate typical remineralization conditions associated with fresh planktonic material (Westrich and Berner, 1984; Middelburg, 1989), however it is possible (especially in the summer) that C_{org} could have been depleted.

4.4 Fe_d fluxes from permeable sands - broader perspective

Even though the TOC and reactive Fe content were relatively low compared to other sediment types, the Fe_d fluxes from the irrigated permeable sediments studied here (>100 μmol Fe m^{-2} d^{-1}) are on a similar order of magnitude to those reported from muddy sediments under a variety of conditions. This includes sediments experiencing high levels of bioirrigation (6000-9000 individuals m^{-2}; Lenstra et al., 2019), overlain by hypoxic or anoxic bottom waters where a breakdown of the surface oxic layer allows for greater fluxes via diffusion or bioturbation (Elrod et al., 2004; Severmann et al., 2010) or from Fe-rich sediments where high Fe-oxide contents and internal Fe-cycling can support extensive Fe reduction, resulting in high concentrations of dissolved Fe in porewater that is released via diffusion, physical mixing, or bioturbation (Wehrmann et al., 2014; Herbert et al., 2021).

Permeable sediments act as biocatalytic filters (Huettel and Rusch, 2000) effectively trapping particulate organic carbon and reactive Fe that is flushed through the sediment (Huettel et al., 1996; Huettel et al., 1998). This promotes carbon remineralization via DIR and the mobilization of diagenetically produced Fe_d. Evidence from our field monitoring suggests seasonal increases (specifically in the late winter and early spring) of reactive Fe content and variations in pyrite concentrations that appear to be, at least partially, driven by inputs of fine-grained material and changes in animal behavior. It is likely that reactive Fe was in part previously released Fe_d that remained in the overlying water of Shinnecock Bay after being rapidly oxidized to colloidal or particulate Fe-oxides (Raiswell and Canfield, 2012; Aller et al., 2023). It was then recaptured by the permeable sand as water was advectively forced through the sediment by animal activity, tidal pumping, currents, and wave action. Again, although the permeable sediments used in our experiments were relatively low in standing stocks of labile C and Fe, there is clear evidence for carbon remineralization and dynamic Fe cycling that supported large Fe_d fluxes in both summer and winter. The slow decrease of the Fe_d flux in the microcosms, independent of the bioirrigation imposed porewater turnover time of ~4 d, demonstrates a requirement for the replenishment of reactive substrates (C_{org}, Fe) in order to sustain high Fe_d release.

While the non-irrigated treatment established in this experiment was intended to be a sedimentary control treatment to estimate geochemical cycling and porewater properties in the absence of advection, it is apparent that without an advective component, the estimated diffusive Fe_d flux is a small fraction of the total potential Fe_d fluxes from these sediments. The estimated flux values from the non-irrigated cores were of similar magnitude to diffusive fluxes reported from muds with fully oxic overlying water (~10 μmol Fe m^{-2} d^{-1}). In our experiments, bioirrigation was the targeted advective component investigated, and was found to have a significant impact on the magnitude of the flux. However, *in situ* there are other advective forcings that may act on permeable sediments to drive fluxes, including waves, tidal forcing, and currents. Recently Charbonnier et al. (2023) reported Fe fluxes of up to 30 μmol Fe m^{-2} d^{-1} from permeable sediments investigated in a lagoon off of the French Mediterranean coast due to the tidal flushing of porewater. Without additional advective components acting on the porewater in these sediments, the Fe_d flux values reported here could therefore largely underestimate the total Fe_d flux from sandy sediments. Future studies should continue to investigate other advective forcings, and potential interactions, on Fe_d fluxes from permeable sediments to further evaluate their role from a global perspective.

5 Conclusions

Overall, porewater Fe_d distributions and cycling suggest the large potential of permeable sandy sediments to support significant benthic Fe fluxes from the seabed in both winter and summer. It is clear that permeable sediments must be considered in global Fe_d flux estimates. Extrapolating our average fluxes from the non-irrigated and irrigated cores suggests Shinnecock Bay (A= 40 km^2) could release ~0.16-1.5 megamoles of Fe throughout a year. Similar sedimentary conditions exist all along the eastern coast of North America (Huettel et al., 2014) including the geographic range of our model organism *C. torquata* (Mangum, 1962), and in large coastal areas of Europe (e.g., the Wadden Sea) and Asia (e.g., the East China Sea). We therefore suggest that similar studies should be performed within this range to continue compiling data on seasonal sedimentary Fe cycling and potential Fe_d fluxes from bioirrigated permeable systems and evaluate if the patterns observed in Shinnecock Bay may hold true in other locations.

Our data suggest that in these permeable sediments, irrigation induced advective porewater flow enhanced transport of reduced constituents, particularly Fe_d, out of the sediment, resulting in significant Fe_d fluxes, ~10x higher than reported Fe_d fluxes from muds used in global models. This suggests any further modeling of Fe_d fluxes, especially in permeable sediments, must explicitly include bioirrigation parameters relevant for dominant species within a specific environment. This may require further testing of

species-specific irrigation patterns. Our flux estimates are high despite fully oxic overlying water conditions, low organic C and reactive Fe contents, suggesting that estimated Fe_d fluxes from bioirrigated permeable sediments may not conform to the previously modeled relationship between carbon oxidation and overlying water oxygen concentration. Future studies should further explore this relationship in geographically diverse permeable sediments, particularly given the biocatalytic filtration function of sands despite relatively low organic carbon and reactive Fe standing stocks.

Data availability statement

The raw data supporting the conclusions of this article will be made available by the authors, without undue reservation.

Author contributions

DS: Data curation, Formal Analysis, Investigation, Writing – original draft, Visualization. ID: Writing – review & editing, Investigation, Methodology, Software. RA: Conceptualization, Funding acquisition, Investigation, Methodology, Writing – review & editing. NV: Conceptualization, Funding acquisition, Investigation, Methodology, Resources, Writing – review & editing. CH: Formal Analysis, Investigation, Writing – review & editing. LW: Conceptualization, Funding acquisition, Investigation, Methodology, Project administration, Resources, Writing – original draft.

Funding

The author(s) declare financial support was received for the research, authorship, and/or publication of this article. This work was supported by NSF Award #1757045. Thank you to Bob Maze and Laurie Landeau for sponsoring graduate student research through the Maze-Landeau Fellowship. LMW also acknowledges funding by a Hanse-Wissenschaftskolleg Fellowship.

Acknowledgments

We would like to thank Katie Wooton and Troy Rasbury from FIRST@Stony Brook for performing the porewater Fe analysis and Greg Henkes and Yang Gao of Stony Brook University for the analysis of total organic carbon.

Conflict of interest

The authors declare that the research was conducted in the absence of any commercial or financial relationships that could be construed as a potential conflict of interest.

Publisher's note

Supplementary material

The Supplementary Material for this article can be found online at: https://www.frontiersin.org/articles/10.3389/fmars.2023.1293893/full#supplementary-material

References

Aller, R. C. (1980). Diagenetic processes near the sediment-water interface of Long Island Sound. II. Fe and Mn. *Adv. Geophys.* 22, 351–415. doi: 10.1016/S0065-2687(08)60068-0

Aller, R. C. (1982). "The effects of macrobenthos on chemical properties of marine sediment and overlying water," in *Animal-sediment relations: the biogenic alteration of sediments*. Eds. P. L. McCall and M. J. S. Trvesz (Boston, MA: Springer), 53–102.

Aller, R. (2001). "Transport and reactions in the bioirrigated zone," in *The benthic boundary layer: transport processes and biogeochemistry*. Eds. B. P. Boudreau and B. B. Jorgensen (Oxford: Oxford University Press).

Aller, R., Dwyer, I., Perger, D. S., Heilbrun, C., Volkenborn, N., and Wehrmann, L. (2023). Estimating benthic Fe and reactive solute fluxes. *Mar. Chem.* 249, 104221. doi: 10.1016/j.marchem.2023.104221

Banta, G. T., Holmer, M., Jensen, M. H., and Kristensen, E. (1999). Effects of two polychaete worms, Nereis diversicolor and Arenicola marina, on aerobic and anaerobic decomposition in a sandy marine sediment. *Aquat. Microbial Ecol.* 19, 189–204. doi: 10.3354/ame019189

Behrenfeld, M. J., Bale, A. J., Kolber, Z. S., Aiken, J., and Falkowski, P. G. (1996). Confirmation of iron limitation of phytoplankton photosynthesis in the equatorial Pacific Ocean. *Nature* 383, 508. doi: 10.1038/383508a0

Behrenfeld, M. J., and Kolber, Z. S. (1999). Widespread iron limitation of phytoplankton in the South Pacific Ocean. *Science* 283, 840–843. doi: 10.1126/science.283.5403.840

Berner, R. A. (1970). Sedimentary pyrite formation. *Am. J. Sci.* 268, 1–23. doi: 10.2475/ajs.268.1.1

Berner, R. A. (1978). Sulfate reduction and the rate of deposition of marine sediments. *Earth Planet. Sci. Lett.* 37, 492–498. doi: 10.1016/0012-821X(78)90065-1

Boudreau, B. P., Huettel, M., Forster, S., Jahnke, R. A., Mclachlan, A., Middelburg, J. J., et al. (2001). Permeable marine sediments: overturning an old paradigm. *EOS Trans. Am. Geophys. Union* 82, 133–136. doi: 10.1029/EO082i011p00133-01

Burdige, D. J. (1991). The kinetics of organic matter mineralization in anoxic marine sediments. *J. Mar. Res.* 49, 727–761. doi: 10.1357/002224091784995710

Canfield, D. E. (1989). Reactive iron in marine sediments. *Geochim. Cosmochim. Acta* 53, 619–632. doi: 10.1016/0016-7037(89)90005-7

Charbonnier, C., Anschutz, P., Tamborski, J., and Van Beek, P. (2023). Benthic fluxes and mineralization processes at the scale of a coastal lagoon: Permeable versus fine-grained sediment contribution. *Mar. Chem.* 254, 104274. doi: 10.1016/j.marchem.2023.104274

Cline, J. D. (1969). Spectrophotometric determination of hydrogen sulfide in natural waters 1. *Limnol. Oceanogr.* 14, 454–458. doi: 10.4319/lo.1969.14.3.0454

Coale, K. H., Johnson, K. S., Fitzwater, S. E., Gordon, R. M., Tanner, S., Chavez, F. P., et al. (1996). A massive phytoplankton bloom induced by an ecosystem-scale iron fertilization experiment in the equatorial Pacific Ocean. *Nature* 383, 495. doi: 10.1038/383495a0

Conway, T. M., and John, S. G. (2014). Quantification of dissolved iron sources to the North Atlantic Ocean. *Nature* 511, 212–215. doi: 10.1038/nature13482

D'Andrea, A. F., Aller, R. C., and Lopez, G. R. (2002). Organic matter flux and reactivity on a South Carolina sandflat: The impacts of porewater advection and macrobiological structures. *Limnol. Oceanogr.* 47, 1056–1070. doi: 10.4319/lo.2002.47.4.1056

D'Andrea, A. F., Lopez, G. R., and Aller, R. C. (2004). Rapid physical and biological particle mixing on an intertidal sandflat. *J. Mar. Res.* 62, 67–92. doi: 10.1357/00222400460744627

Dale, A. W., Nickelsen, L., Scholz, F., Hensen, C., Oschlies, A., and Wallmann, K. (2015). A revised global estimate of dissolved iron fluxes from marine sediments. *Global Biogeochem. Cycles* 29, 691–707. doi: 10.1002/2014GB005017

Davis, R. B. (1974). Tubificids alter profiles of redox potential and pH in profundal lake sediment 1. *Limnol. Oceanogr.* 19, 342–346. doi: 10.4319/lo.1974.19.2.0342

de Beer, D., Wenzhöfer, F., Ferdelman, T. G., Boehme, S. E., Huettel, M., Van Beusekom, J. E., et al. (2005). Transport and mineralization rates in North Sea sandy intertidal sediments, Sylt-Rømø basin, Wadden Sea. *Limnol. Oceanogr.* 50, 113–127. doi: 10.4319/lo.2005.50.1.0113

Dobbs, F. C., and Whitlatch, R. B. (1982). Aspects of deposit-feeding by the polychaete Clymenella torquata. *Ophelia* 21, 159–166. doi: 10.1080/00785326.1982.10426584

Elrod, V. A., Berelson, W. M., Coale, K. H., and Johnson, K. S. (2004). The flux of iron from continental shelf sediments: A missing source for global budgets. *Geophys. Res. Lett.* 31, L12307. doi: 10.1029/2004GL020216

Forster, S., and Graf, G. (1995). Impact of irrigation on oxygen flux into the sediment: intermittent pumping by Callianassa subterranea and "piston-pumping" by Lanice conChilega. *Mar. Biol.* 123, 335–346. doi: 10.1007/BF00353625

Forster, S., Huettel, M., and Ziebis, W. (1996). Impact of boundary layer flow velocity on oxygen utilisation in coastal sediments. *Mar. Ecol. Prog. Ser.* 143, 173–185. doi: 10.3354/meps143173

Fossing, H., and Jørgensen, B. B. (1989). Measurement of bacterial sulfate reduction in sediments: evaluation of a single-step chromium reduction method. *Biogeochemistry* 8, 205–222. doi: 10.1007/BF00002889

Froelich, P. N., Klinkhammer, G. P., Bender, M. L., Luedtke, N. A., Heath, G. R., Cullen, D., et al. (1979). Early oxidation of organic matter in pelagic sediments of eastern equitorial Atlantic: suboxic diagenesis. *Geochimica Cosmochima Acta* 43, 1075–1090. doi: 10.1016/0016-7037(79)90095-4

Green, M. A., Gulnick, J. D., Dowse, N., and Chapman, P. (2004). Spatiotemporal patterns of carbon remineralization and bio-irrigation in sediments of Casco Bay Estuary, Gulf of Maine. *Limnol. oceanogr.* 49, 396–407. doi: 10.4319/lo.2004.49.2.0396

Gudasz, C., Bastviken, D., Steger, K., Premke, K., Sobek, S., and Tranvik, L. J. (2010). Temperature-controlled organic carbon mineralization in lake sediments. *Nature* 466, 478–481. doi: 10.1038/nature09186

Herbert, L. C., Zhu, Q., Michaud, A. B., Laufer-meiser, K., Jones, C. K., Riedinger, N., et al. (2021). Benthic iron flux influenced by climate-sensitive interplay between organic carbon availability and sedimentation rate in Arctic fjords. *Limnol. Oceanogr.* 66, 3374–3392. doi: 10.1002/lno.11885

Hu, G., Dam-Johansen, K., Wedel, S., and Hansen, J. P. (2006). Decomposition and oxidation of pyrite. *Prog. Energy combustion Sci.* 32, 295–314. doi: 10.1016/j.pecs.2005.11.004

Huettel, M. (1990). Influence of the lugworm Arenicola marina on porewater nutrient profiles of sand flat sediments. *Mar. Ecol. Prog. series. Oldendorf.* 62, 241–248. doi: 10.3354/meps062241

Huettel, M., Berg, P., and Kostka, J. E. (2014). Benthic exchange and biogeochemical cycling in permeable sediments. *Ann. Rev. Mar. Sci.* 6, 23–51. doi: 10.1146/annurev-marine-051413-012706

Huettel, M., and Rusch, A. (2000). Transport and degradation of phytoplankton in permeable sediment. *Limnol. Oceanogr.* 45, 534–549. doi: 10.4319/lo.2000.45.3.0534

Huettel, M., Ziebis, W., and Forster, S. (1996). Flow-induced uptake of particulate matter in permeable sediments. *Limnol. Oceanogr.* 41, 309–322. doi: 10.4319/lo.1996.41.2.0309

Huettel, M., Ziebis, W., Forster, S., and Luther, G. III (1998). Advective transport affecting metal and nutrient distributions and interfacial fluxes in permeable sediments. *Geochimica Cosmochimica Acta* 62, 613–631. doi: 10.1016/S0016-7037(97)00371-2

Jahnke, R., Richards, M., Nelson, J., Robertson, C., Rao, A., and Jahnke, D. (2005). Organic matter remineralization and porewater exchange rates in permeable South Atlantic Bight continental shelf sediments. *Continental Shelf Res.* 25, 1433–1452. doi: 10.1016/j.csr.2005.04.002

Janssen, F., Huettel, M., Meyer, V., and Witte, U. (2005). Pore-water advection and solute fluxes in permeable marine sediments (I): Calibration and performance of the novel benthic chamber system Sandy. *Limnol. Oceanogr.* 50, 768–778. doi: 10.4319/lo.2005.50.3.0768

Jickells, T. D., and Rae, J. E. (2005). *Biogeochemistry of intertidal sediments* (Cambridge, UK: Cambridge University Press).

Jorgensen, B. B. (1978). A comparison of methods for the quantification of bacterial sulfate reduction in coastal marine sediments. *Geomicrobiol. J.* 1, 11–27. doi: 10.1080/01490457809377723

Klump, J. V., and Martens, C. S. (1989). The seasonality of nutrient regeneration in an organic-rich coastal sediment: Kinetic modeling of changing pore-water nutrient and sulfate distributions. *Limnol. Oceanogr.* 34, 559–577. doi: 10.4319/lo.1989.34.3.0559

Koretsky, C. M., Moore, C. M., Lowe, K. L., Meile, C., Dichristina, T. J., and Van Cappellen, P. (2003). Seasonal oscillation of microbial iron and sulfate reduction in saltmarsh sediments (Sapelo Island, GA, USA). *Biogeochemistry* 64, 179–203. doi: 10.1023/A:1024940132078

Kostka, J. E., and Luther, G. W.III (1994). Partitioning and speciation of solid phase iron in saltmarsh sediments. *Geochimica Cosmochimica Acta* 58, 1701–1710. doi: 10.1016/0016-7037(94)90531-2

Kristensen, E. (2001). Impact of polychaetes (Nereis spp. and Arenicola marina) on carbon biogeochemistry in coastal marine sedimentsPresented during the ACS Division of Geochemistry symposium 'Biogeochemical Consequences of Dynamic Interactions Between Benthic Fauna, Microbes and Aquatic Sediments', San Diego, April 2001. *Geochemical Trans.* 2, 92–103. doi: 10.1039/B108114D

Kristensen, E., and Kostka, J. (2005). Macrofaunal burrows and irrigation in marine sediment: microbiological and biogeochemical interactions. *Interact. between macro- and microorganisms Mar. sediments* 60, 125–157. doi: 10.1029/CE060p0125

Kristensen, E., Penha-Lopes, G., Delefosse, M., Valdemarsen, T., Quintana, C. O., and Banta, G. T. (2012). What is bioturbation? The need for a precise definition for fauna in aquatic sciences. *J. Mar. Ecol. Prog. Ser.* 446, 285–302. doi: 10.3354/meps09506

Lenstra, W. K., Hermans, M., Séguret, M. J., Witbaard, R., Behrends, T., Dijkstra, N., et al. (2019). The shelf-to-basin iron shuttle in the Black Sea revisited. *Chem. Geology* 511, 314–341. doi: 10.1016/j.chemgeo.2018.10.024

Lenstra, W. K., Hermans, M., Séguret, M. J., Witbaard, R., Severmann, S., Behrends, T., et al. (2021). Coastal hypoxia and eutrophication as key controls on benthic release and water column dynamics of iron and manganese. *Limnol. Oceanogr.* 66 (3), 807–826. doi: 10.1002/lno.11644

Liu, J., Pellerin, A., Antler, G., Kasten, S., Findlay, A. J., Dohrmann, I., et al. (2020). Early diagenesis of iron and sulfur in Bornholm Basin sediments: The role of near-surface pyrite formation. *Geochimica Cosmochimica Acta* 284, 43–60. doi: 10.1016/j.gca.2020.06.003

Lovley, D. R. (1997). Microbial Fe(III) reduction in subsurface environments. *FEMS Microbiol. Rev.* 20, 305–313. doi: 10.1111/j.1574-6976.1997.tb00316.x

Lovley, D. R., and Phillips, E. J. (1986). Organic matter mineralization with reduction of ferric iron in anaerobic sediments. *Appl. Environ. Microbiol.* 51, 683–689. doi: 10.1128/aem.51.4.683-689.1986

Lovley, D. R., and Phillips, E. J. (1988). Manganese inhibition of microbial iron reduction in anaerobic sediments. *Geomicrobiol. J.* 6, 145–155. doi: 10.1080/01490458809377834

Luther, III, G. W. (1987). Pyrite oxidation and reduction: molecular orbital theory considerations. *Geochimica Cosmochimica Acta* 51, 3193–3199. doi: 10.1016/0016-7037(87)90127-X

Luther, III, G. W. (1991). Pyrite synthesis via polysulfide compounds. *Geochimica Cosmochimica Acta* 55, 2839–2849. doi: 10.1016/0016-7037(91)90449-F

Luther, III, G. W., Giblin, A., Howarth, R. W., and Ryans, R. A. (1982). Pyrite and oxidized iron mineral phases formed from pyrite oxidation in salt marsh and estuarine sediments. *Geochimica Cosmochimica Acta* 46, 2665–2669. doi: 10.1016/0016-7037(82)90385-4

Mangum, C. P. (1962). Studies on speciation in maldanid polychaetes of the North American Atlantic coast. *I. A taxonomic revision three species subfamily Euclymeninae* 65, 12. doi: 10.1016/0010-406X(63)90232-9

Mangum, C. P. (1964). Studies on speciation in maldanid polychaetes of the north american atlantic coast. ii. distribution and competitive interaction of five sympatric species 1. *Limnol. Oceanogr.* 9, 12–26. doi: 10.4319/lo.1964.9.1.0012

Martin, J. H., and Fitzwater, S. E. (1988). Iron deficiency limits phytoplankton growth in the north-east Pacific subarctic. *Nature* 331, 341. doi: 10.1038/331341a0

Martin, W., and Sayles, F. (1987). Seasonal cycles of particle and solute transport processes in nearshore sediments: 222Rn226Ra and 234Th238U disequilibrium at a site in Buzzards Bay, MA. *Geochimica Cosmochimica Acta* 51, 927–943. doi: 10.1016/0016-7037(87)90106-2

Matsui, G., Volkenborn, N., Polerecky, L., Henne, U., Wethey, D., Lovell, C., et al. (2011). Mechanical imitation of bidirectional bioadvection in aquatic sediments. *Limnol. Oceanogr.: Methods* 9, 84–96. doi: 10.4319/lom.2011.9.84

Meysman, F. J., Galaktionov, O. S., Gribsholt, B., and Middelburg, J. J. (2006). Bioirrigation in permeable sediments: Advective pore-water transport induced by burrow ventilation. *Limnol. Oceanogr.* 51, 142–156. doi: 10.4319/lo.2006.51.1.0142

Michaud, A. B., Laufer, K., Findlay, A., Pellerin, A., Antler, G., Turchyn, A. V., et al. (2020). Glacial influence on the iron and sulfur cycles in Arctic fjord sediments (Svalbard). *Geochimica Cosmochimica Acta* 280, 423–440. doi: 10.1016/j.gca.2019.12.033

Middelburg, J. J. (1989). A simple rate model for organic matter decomposition in marine sediments. *Geochimica Cosmochimica Acta* 53 (7), 1577–1581. doi: 10.1016/0016-7037(89)90239-1

Millero, F. J. (1991). The oxidation of H2S in Black Sea waters. *Deep Sea Res. Part A. Oceanographic Res. Papers* 38, S1139–S1150. doi: 10.1016/S0198-0149(10)80028-7

Millero, F. J., Yao, W., and Aicher, J. (1995). The speciation of Fe (II) and Fe (III) in natural waters. *Mar. Chem.* 50, 21–39. doi: 10.1016/0304-4203(95)00024-L

Na, T., Gribsholt, B., Galaktionov, O. S., Lee, T., and Meysman, F. J. (2008). Influence of advective bio-irrigation on carbon and nitrogen cycling in sandy sediments. *J. Mar. Res.* 66, 691–722. doi: 10.1357/002224008787536826

Nielsen, L. P., and Risgaard-Petersen, N. (2015). Rethinking sediment biogeochemistry after the discovery of electric currents. *Annu. Rev. Mar. Sci.* 7, 425–442. doi: 10.1146/annurev-marine-010814-015708

Pomeroy, L. R., and Wiebe, W. J. (2001). Temperature and substrates as interactive limiting factors for marine heterotrophic bacteria. *Aquat. Microbial. Ecol.* 23, 187–204. doi: 10.3354/ame023187

Poulton, S. W., and Canfield, D. E. (2005). Development of a sequential extraction procedure for iron: implications for iron partitioning in continentally derived particulates. *Chem. Geol.* 214, 209–221. doi: 10.1016/j.chemgeo.2004.09.003

Poulton, S. W., Krom, M. D., and Raiswell, R. (2004). A revised scheme for the reactivity of iron (oxyhydr) oxide minerals towards dissolved sulfide. *Geochimica cosmochimica Acta* 68, 3703–3715. doi: 10.1016/j.gca.2004.03.012

Precht, E., Franke, U., Polerecky, L., and Huettel, M. (2004). Oxygen dynamics in permeable sediments with wave-driven pore water exchange. *Limnol. Oceanogr.* 49, 693–705. doi: 10.4319/lo.2004.49.3.0693

Pyzik, A. J., and Sommer, S. E. (1981). Sedimentary iron monosulfides: kinetics and mechanism of formation. *Geochimica Cosmochimica Acta* 45, 687–698. doi: 10.1016/0016-7037(81)90042-9

Quintana, C. O., Shimabukuro, M., Pereira, C. O., Alves, B. G., Moraes, P. C., Valdemarsen, T., et al. (2015). Carbon mineralization pathways and bioturbation in coastal Brazilian sediments. *Sci. Rep.* 5, 1–13. doi: 10.1038/srep16122

Raiswell, R., and Canfield, D. E. (2012). The iron biogeochemical cycle past and present. *Geochemical Perspect.* 1, 1–2. doi: 10.7185/geochempersp.1.1

Reimers, C. E., Stecher, H. A.III, Taghon, G. L., Fuller, C. M., Huettel, M., Rusch, A., et al. (2004). *In situ* measurements of advective solute transport in permeable shelf sands. *Continental shelf Res.* 24, 183–201. doi: 10.1016/j.csr.2003.10.005

Rhoads, D. C. (1967). Biogenic reworking of intertidal and subtidal sediments in Barnstable Harbor and Buzzards Bay, Massachusetts. *J. Geology* 75, 461–476. doi: 10.1086/627272

Rhoads, D. C., and Stanley, D. J. (1965). Biogenic graded bedding. *J. Sedimentary Res.* 35, 956–963. doi: 10.1306/74D713BB-2B21-11D7-8648000102C1865D

Rickard, D. (2006). The solubility of feS. *Geochimica Cosmochimica Acta* 70, 5779–5789. doi: 10.1016/j.gca.2006.02.029

Rickard, D., and Luther, G. W. (2007). Chemistry of iron sulfides. *Chem. Rev.* 107, 514–562. doi: 10.1021/cr0503658

Rowe, G., Theroux, R., Phoel, W., Quinby, H., Wilke, R., Koschoreck, D., et al. (1988). Benthic carbon budgets for the continental shelf south of New England. *Continental Shelf Res.* 8, 511–527. doi: 10.1016/0278-4343(88)90066-0

Santos, I. R., Eyre, B. D., and Huettel, M. (2012). The driving forces of porewater and groundwater flow in permeable coastal sediments: A review. *Estuarine Coast. Shelf Sci.* 98, 1–15. doi: 10.1016/j.ecss.2011.10.024

Sarazin, G., Michard, G., and Prevot, F. (1999). A rapid and accurate spectroscopic method for alkalinity measurements in sea water samples. *Water Res.* 33, 290–294. doi: 10.1016/S0043-1354(98)00168-7

Schippers, A., and Jørgensen, B. B. (2001). Oxidation of pyrite and iron sulfide by manganese dioxide in marine sediments. *Geochimica Cosmochimica Acta* 65, 915–922. doi: 10.1016/S0016-7037(00)00589-5

Schlüter, M., Sauter, E., Hansen, H.-P., and Suess, E. (2000). Seasonal variations of bioirrigation in coastal sediments: modelling of field data. *Geochimica Cosmochimica Acta* 64, 821–834. doi: 10.1016/S0016-7037(99)00375-0

Scholz, F., McManus, J., Mix, A. C., Hensen, C., and Schneider, R. R. (2014). The impact of ocean deoxygenation on iron release from continental margin sediments. *Nat. Geosci.* 7 (6), 433–437. doi: 10.1038/ngeo2162

Schoonen, M., and Barnes, H. (1991). Reactions forming pyrite and marcasite from solution: II. Via FeS precursors below 100 C. *Geochimica Cosmochimica Acta* 55, 1505–1514. doi: 10.1016/0016-7037(91)90123-M

Seeberg-Elverfeldt, J., Schlüter, M., Feseker, T., and Kölling, M. (2005). Rhizon sampling of porewaters near the sediment-water interface of aquatic systems. *Limnol. oceanogr.: Methods* 3, 361–371. doi: 10.4319/lom.2005.3.361

Seibert, S. L., Böttcher, M. E., Schubert, F., Pollmann, T., Giani, L., Tsukamoto, S., et al. (2019). Iron sulfide formation in young and rapidly-deposited permeable sands at the land-sea transition zone. *Sci. total Environ.* 649, 264–283. doi: 10.1016/j.scitotenv.2018.08.278

Severmann, S., Mcmanus, J., Berelson, W. M., and Hammond, D. E. (2010). The continental shelf benthic iron flux and its isotope composition. *Geochimica Cosmochimica Acta* 74, 3984–4004. doi: 10.1016/j.gca.2010.04.022

Solorzano, L. (1969). determination of ammonia in natural waters by the phenolhypochlorite method 1 1 This research was fully supported by US Atomic Energy Commission Contract No. ATS (11-1) GEN 10, PA 20. *Limnol. oceanogr.* 14, 799–801. doi: 10.4319/lo.1969.14.5.0799

Steiner, Z., Lazar, B., Erez, J., and Turchyn, A. V. (2018). Comparing Rhizon samplers and centrifugation for pore-water separation in studies of the marine carbonate system in sediments. *Limnol. Oceanogr.: Methods* 16, 828–839. doi: 10.1002/lom3.10286

Stookey, L. L. (1970). Ferrozine—a new spectrophotometric reagent for iron. *Analytical Chem.* 42, 779–781. doi: 10.1021/ac60289a016

van de Velde, S., and Meysman, F. J. (2016). The influence of bioturbation on iron and sulphur cycling in marine sediments: a model analysis. *J. Aquat. Geochem.* 22, 469–504. doi: 10.1007/s10498-016-9301-7

Viollier, E., Inglett, P., Hunter, K., Roychoudhury, A., and van Cappellen, P. (2000). The ferrozine method revisited: Fe (II)/Fe (III) determination in natural waters. *Appl. geochem.* 15, 785–790. doi: 10.1016/S0883-2927(99)00097-9

Volkenborn, N., Hedtkamp, S., van Beusekom, J., and Reise, K. (2007a). Effects of bioturbation and bioirrigation by lugworms (Arenicola marina) on physical and chemical sediment properties and implications for intertidal habitat succession. *Estuarine Coast. Shelf Sci.* 74, 331–343. doi: 10.1016/j.ecss.2007.05.001

Volkenborn, N., Meile, C., Polerecky, L., Pilditch, C. A., Norkko, A., Norkko, J., et al. (2012). Intermittent bioirrigation and oxygen dynamics in permeable sediments: An experimental and modeling study of three tellinid bivalves. *J. Mar. Res.* 70, 794–823. doi: 10.1357/002224012806770955

Volkenborn, N., Polerecky, L., Hedtkamp, S., van Beusekom, J. E., and de Beer, D. (2007b). Bioturbation and bioirrigation extend the open exchange regions in permeable sediments. *Limnol. Oceanogr.* 52, 1898–1909. doi: 10.4319/lo.2007.52.5.1898

Volkenborn, N., Woodin, S. A., Wethey, D. S., and Polerecky, L. (2019). "Bioirrigation," in *Encyclopedia of ocean sciences*, *3rd ed.* Eds. J. K. Cochran, H. J. Bokuniewicz and P. L. Yager (Amsterdam, The Netherlands: Elsevier), 663–670.

Wehrmann, L. M., Formolo, M. J., Owens, J. D., Raiswell, R., Ferdelman, T. G., Riedinger, N., et al. (2014). Iron and manganese speciation and cycling in glacially influenced high-latitude fjord sediments (West Spitsbergen, Svalbard): evidence for a benthic recycling-transport mechanism. *Geochimica Cosmochimica Acta* 141, 628–655. doi: 10.1016/j.gca.2014.06.007

Wendelboe, K., Egelund, J. T., Flindt, M. R., and Valdemarsen, T. (2013). Impact of lugworms (Arenicola marina) on mobilization and transport of fine particles and organic matter in marine sediments. *J. sea Res.* 76, 31–38. doi: 10.1016/j.seares.2012.10.013

Westrich, J. T., and Berner, R. A. (1984). The role of sedimentary organic matter in bacterial sulfate reduction: The G model tested 1. *Limnol. oceanogr.* 29, 236–249. doi: 10.4319/lo.1984.29.2.0236

Wethey, D. S., Woodin, S. A., Volkenborn, N., and Reise, K. (2008). Porewater advection by hydraulic activities of lugworms, Arenicola marina: a field, laboratory and modeling study. *J. Mar. Res.* 66, 255–273. doi: 10.1357/002224008785837121

Wilkin, R., and Barnes, H. (1996). Pyrite formation by reactions of iron monosulfides with dissolved inorganic and organic sulfur species. *Geochimica Cosmochimica Acta* 60, 4167–4179. doi: 10.1016/S0016-7037(97)81466-4

Wilson, A. M., Huettel, M., and Klein, S. (2008). Grain size and depositional environment as predictors of permeability in coastal marine sands. *Estuarine Coast. Shelf Sci.* 80, 193–199. doi: 10.1016/j.ecss.2008.06.011

Zopfi, J., Ferdelman, T., and Fossing, H. (2004). "Distribution and fate of sulfur intermediates–sulfite, thiosulfate, and elemental sulfur–in marine sediments," in *Sulfur biogeochemistry–Past and present* (Boulder, Colorado: Geological Society of America). doi: 10.1130/0-8137-2379-5